Simulating the evolution of the Asian and African monsoons during the past 30 Myr using an atmospheric general circulation model

Frédéric Fluteau, Gilles Ramstein, Jean Besse

JOURNAL OF GEOPHYSICAL RESEARCH, VOL. 104, NO. D10, PAGES 11,995–12,018, MAY 27, 1999

Simulating the evolution of the Asian and African monsoons during the past 30 Myr using an atmospheric general circulation model

Frédéric Fluteau,[1,2] G. Ramstein,[2] and Jean Besse[1]

Abstract. At geologic timescales, many proxy data suggest a contrasting evolution of Asian and African monsoons since the Oligocene. The Asian summer monsoon increases drastically around 8 Ma, whereas the African summer monsoon gradually weakens during the Miocene. Using an atmospheric general circulation model, we simulate most of the spatial evolutions of both monsoons only accounting for the changes of paleogeography, including continental drift, orogeny, and sea level change. The paleogeographic changes modify drastically the climate over central and southern Asia between the Oligocene and the present. The retreat of an epicontinental sea warms central Eurasia in summer. The heating of this area and the uplifts of the Tibetan plateau and of the Himalayas deepen the Asian low-pressure cell and displace it northwest. This then shifts precipitation from Indochina toward the southern flank of the Himalayas. This is in good agreement with proxy data. Therefore our modeling studies support a shift and a strengthening of the Asian monsoon during the late Tertiary rather than a real "onset". We suggest that the increase in seasonal precipitation and the strengthening of the number of days with heavy rainfall over the Himalayas from 30 Ma to the present may be of critical importance to explain the long- term evolution of physical erosion of this area. We also investigate the respective impact of the Paratethys shrinkage and of the Tibetan plateau uplift through sensitivity experiments and prove that the Paratethys retreat plays an important role in monsoon evolution. The northward drift of the African continent confines summer monsoon precipitation to a thin belt which favors the stretching of the subtropical desert, in good agreement with data. We finally show that during the Oligocene, the African and Asian monsoon systems are clearly separated by the Tethys seaway. The closure of this seaway and the evolution of the Asian monsoon induce a connection between both monsoon systems in the low and middle troposphere.

1. Introduction

The monsoon dominates the large-scale tropical circulation on both the African and Southeast Asian continents. It results from the thermal contrast between the continent and the surrounding ocean [*Hastenrath*, 1985; *Webster*, 1987]. In winter, the continent is colder than the ocean and induces northeasterly winds toward the Arabian Sea (Asian monsoon) and toward the Gulf of Guinea (African monsoon), producing weak precipitation because of the little moisture brought by these atmospheric masses [*Hastenrath*, 1985]. In summer, overheated continents become warmer than the ocean. A low-pressure cell is then generated over the warm continents, and a high-pressure cell over the cold ocean. This differential heating induces advection of moist air, producing heavy precipitation in a tropical belt stretching across Africa, India, and Southeast Asia. The release of a huge amount of latent heat contributes to the strengthening of the monsoon circulation [*Hastenrath*, 1985; *Webster*, 1987]. Although driven by a common mechanism, the rainfall intensity of the Asian monsoon is stronger than that of the African monsoon. This difference is due to the Asian continental size and to the presence of orography (Tibetan plateau and Himalayan range) [*James*, 1994].

Monsoons present a large time variability, ranging from years to thousands of years and more [*Prell et al.*, 1992]. At geologic timescales (more than a million years), paleoclimatic indicators suggest an abrupt strengthening of the Asian monsoon during the late Miocene, about 7.5 Ma [*Quade et al.*, 1989; *Prell et al.*, 1992]. Although sparse, paleoclimatic indicators suggest the development of a subtropical desert over northern Africa to the detriment of the monsoon [*Axelrod and Raven*, 1978; *Ruddiman et al.*, 1989; *Maley*, 1996].

At geologic timescales, monsoon evolution may be influenced by different forcing factors such as paleogeographic changes, oceanic circulation changes, variations of carbon dioxide concentration and variations in insolation [*Barron and Washington*, 1984; *Frakes et al.*, 1992]. The impact of some of these forcing factors was investigated through numerical experiments using an atmospheric general circulation model (AGCM) [*Barron and Washington*, 1984; *Kutzbach et al.*, 1989; *Ramstein et al.*, 1997a].

Until now, most experiments on the monsoon have focused on the impact of a mountain uplift without accounting for changes in plate motions or sea-land distribution. Sensitivity experiments to the Himalayan and Tibetan uplift were done using full or half

[1]Laboratoire de Paléomagnétisme et Géodynamique, Institut de Physique du Globe de Paris.

[2]Laboratoire des Sciences du Climat et de l'Environnement, CE-Saclay.

Paper number 1999JD900048.
0148-0227/99/1999JD900048$09.00

altitude of the mountain ranges in a present day environment [*Kutzbach et al.*, 1989; *Ruddiman and Kutzbach*, 1989; *Prell and Kutzback*, 1992; *Kutzbach et al.*, 1993]. Major results were that the uplift of the Tibetan plateau significantly increases the Asian monsoon intensity over most of southern Asia (+50% in summer precipitation) [*Prell and Kutzbach*, 1992] and modifies the climate over adjacent areas (Siberia, central Asia, Middle East, Mediterranean basin) [*Kutzbach et al.*, 1989; *Ruddiman and Kutzbach*, 1989].

Other factors such as atmospheric carbon dioxide concentration, oceanic circulation, and orbital parameters influence the climate. The atmospheric carbon dioxide plays a significant role. The modeling curve of *Berner* [1992] points out an atmospheric CO_2 concentration doubled with respect to the present day in the past 30 Myr. *Prell and Kutzbach* [1992] showed that a CO_2 doubling enhances monsoon precipitation by only 7%. Conversely, this CO_2 doubling could lead to a 6°C warming at middle and high latitudes [*Ruddiman et al.*, 1997a].

Oceanic circulation patterns are induced by the evolution of oceanic basins and the closure or opening of seaways (another consequence of plate motions). Despite tectonic drift, the major features of the oceanic circulation in the late Cenozoic were relatively similar to present day circulation. A thermohaline oceanic circulation began to be established during the early Miocene [*Kennett and Scott*, 1990]. Oxygen isotopic analyses show a weak cooling of sea surface temperature (SST) at high latitudes during the late Tertiary but hardly any changes in SST occurred in the tropics [*Frakes et al.*, 1994]. Finally, using an AGCM coupled with a mixed oceanic layer allowing to take into account the thermal response of the ocean [*Ramstein et al.*, 1997a], we have shown that the changes in SST for these periods were not inducing drastic modification compared to paleogeographic changes.

The changes in insolation at the top of the atmosphere are driven by orbital parameters of Earth and solar constant. However, we are not able to predict their values beyond 5 Myr [*Laskar*, 1988]. Moreover, the fluctuations of these parameters vary on a timescale shorter than the evolutions of the Asian and African monsoons depicted here. Thus we do not change the orbital parameters in our simulations.

Among the causes driving climate changes during the late Cenozoic, we will focus on the impact of the paleogeographic changes on the Asian and African monsoons using an AGCM.

During the late Cenozoic, orogenic episodes formed the great mountain ranges and plateaus (Tibet, Himalayas, Andes, Rockies, Alps) observed today. Also during this time, significant changes occurred in the land-sea distribution such as the shrinkage of the Paratethys Sea, an epicontinental sea stretching from Europe to western Siberia, and the closure of the Tethys seaway. We will investigate the climatic impact of the paleogeography of the Oligocene (30 Myr ago) and the middle late Miocene (10 Myr ago). These periods represent two different states in the Tibetan and Himalayan uplifts. We have also analyzed the respective impact of Paratethys shrinkage and Tibetan plateau uplift through sensitivity experiments.

2. Paleogeographic Reconstruction

2.1. Plate Reconstruction

Plate reconstruction (Figures 1a and 1b) was established using the procedure described by *Besse and Courtillot* [1988]. Oceanic kinematic parameters are first used to place the major continents in their relative positions. For this, we use the finite reconstruction parameters of *Olivet et al.* [1984] for the North and Central Atlantic Ocean, of *Nürnberg and Muller* [1991] for the South Atlantic Ocean, and of *Royer and Sandwell* [1989] for the Indian Ocean. The paleomagnetic synthetic apparent polar wander paths (APWPs) of *Besse and Courtillot* [1991] were then used to fix the paleolatitude grid. These APWPs were constructed from a careful selection of the best paleomagnetic poles available for Asia, Europe, America, and Africa, transferred onto a single reference frame and averaged over 20 Myr time windows. In each of these independent windows, data from individual plates are almost always found to be in agreement, which verifies the quality of the original paleomagnetic data, the cinematic models, and the axial dipole assumption. The 20 Ma sequences of paleomagnetic poles define a "synthetic" APWP, in excellent agreement with the "classical" paths from each plate. The 95% level uncertainties on pole positions are of the order of 3° for the 10 and 30 Ma poles, leading to rather well constrained paleolatitudes.

The hot-spot reference frame [*Morgan*, 1983] was not used because significant inter-hot spot motion [*Chase*, 1983; *Molnar and Stock*, 1987] and true polar wander [*Besse and Courtillot*, 1991] cast some doubt on the use of this method as a global reconstruction tool.

The procedure described above can be used as long as continents are not strongly deformed, or separated by destructive active margins. This is, of course, not the case for the regions bordering the Tethys, where a collision has occurred since the end of the Mesozoic. In particular, central and southeast Asia are characterized by intense deformation linked to the Indian-Asian collision. Since the collision of India with Eurasia at about 50 Ma, roughly north-south intracontinental convergence has occurred at a rate of around 5 cm/yr. A combined analysis of magnetic anomalies from the Indian Ocean [*Patriat and Achache*, 1984] with paleomagnetic data on the northern edge of India and southern edge of Eurasia [*Achache et al.*, 1984; *Besse et al.*, 1984; *Chen et al.*, 1993] has shown a N-S convergence in excess of 2600 km. The paleomagnetic studies on Cretaceous rocks from Tarim [*Li*, 1990], the Junggar block, and Tibet (for a review, see *Chen et al.* [1993]) indicate distributed deformation during the Tertiary within central Asia and confirm the total amplitude of convergence. The relative motion of India with respect to Siberia is well constrained by the classical cinematic plate circuit Asia-North America-Africa-India using the North and Central Atlantic and the Indian Ocean, respectively. The paleoposition of the Indochina block, expulsed southward during the collision, is restored using the South China Sea kinematics parameters of *Briais et al.* [1993].

2.2. Land-Sea Distribution

We restored the paleoshorelines, using mainly the geologic maps of the Tethys program [*Dercourt et al.*, 1993]. Changes in the distribution of seas were not only due to global eustatic sea level fluctuations [*Haq*, 1984], but also to the major orogenic phases which occurred along the southern Eurasian margin in response to the convergence of Arabia and Africa, resulting in the buildup of major mountain chains spanning from the Alps to Zagros. The collision between Arabia and Eurasia closed a seaway connecting the Indian and Atlantic Oceans during the early Miocene. Another major feature of the late Tertiary period is the shrinkage of the Paratethys epicontinental sea in Europe and Asia [*Dercourt et al.*, 1993]. We have therefore reproduced a

a) 30 Ma paleogeography

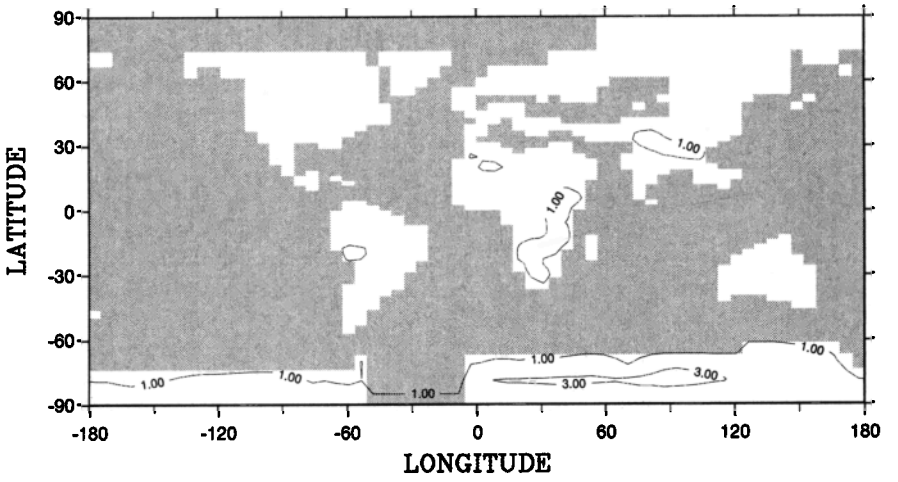

b) 10 Ma paleogeography

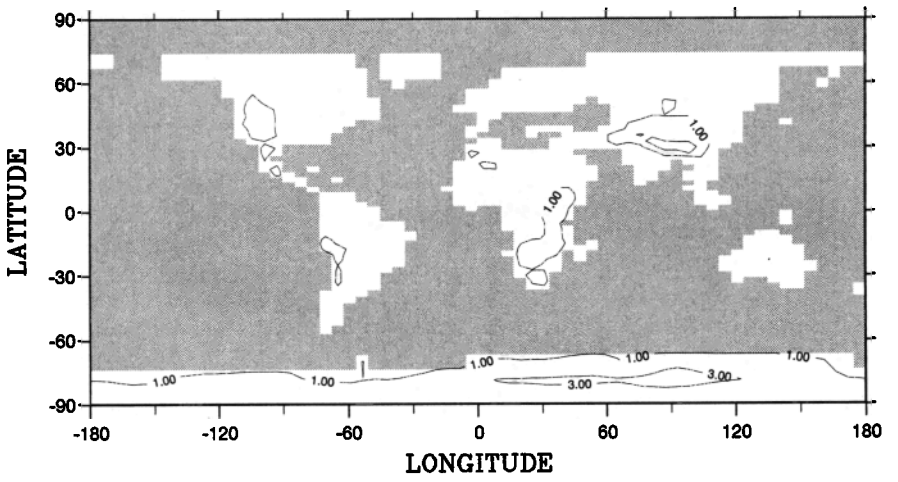

c) PD geography

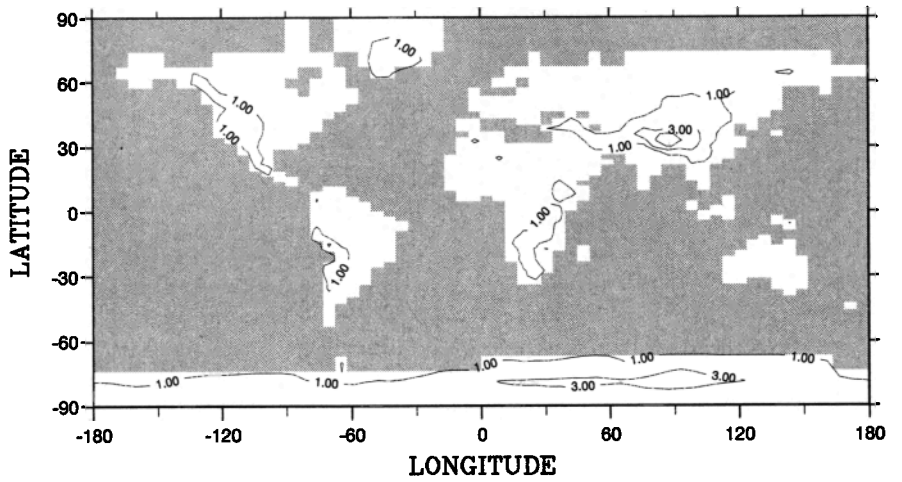

Figure 1. Paleogeographic reconstructions at (a) 30 Ma, (b) 10 Ma, and (c) PD. Isolines are for 1 km, 3 km, and 5 km. Gray area represents oceans. The figures are represented at our model resolution.

large Paratethys sea in our Oligocene reconstruction stretching from Europe to western Siberia (Figure 1a), as shown in the Oligocene Tethys paleogeographic map of *Lorenz et al.* [1993].

During the Miocene, tectonic activity and eustatic changes contributed to the shrinkage of the Paratethys sea, which was localized in a confined area of central Eurasia (Figure 1b) (Alpine-Carpathian and Ponto-Caspian basins) until the middle Miocene [*Orszag-Sperber et al.*, 1993]. Pathways connecting this inland sea with open oceans were progressively closed in response to the evolution of the Alpine-Carpathian-Dinaridic orogenic belt [*Rögl and Steininger*, 1984; *Sztano*, 1995]. Sea level regression further isolated the Paratethys Sea during some short periods, favoring the onset of endemic faunas [see *Sztano*, 1995, Figure 2]. The last connection with the Mediterranean Sea occurred between the late Burdigalian (18 Ma) up to the middle Seravallian (14 Ma) through the Slovenian corridor [*Nagymarosy*, 1990, in *Sztano*, 1995], whereas the marine connection with the Indian Ocean was already closed since the late early Miocene (18 Ma) [*Rögl and Steininger*, 1984]. Thus, during the middle Miocene (14 Ma), the Paratethys Sea became entirely isolated, the salinity decreased by about 30%, and endemic fauna appeared [*Hallam*, 1994]. In the 10 Ma reconstruction, we only consider the deeper basins and the flooding zones represented by shallow lacustrine sediment deposits [*Orszag-Sperber et al.*, 1993] (Figure 1b).

2.3. Topography

The deformation of Asia and the Tibetan plateau have been the subject of an ongoing controversy over the last decade. End-member models involve crustal or lithosphere doubling [*Powell and Conoghan*, 1975; *Barazangi and Ni*, 1982], homogeneous crustal or lithospheric thickening [*Houseman and England*, 1986a, 1986b], inhomogeneous strain concentrated along a few major mountain ranges, or sutures or strike-slip faulting leading to lateral escape of blocks [*Tapponnier et al.*, 1986; *Peltzer and Tapponnier*, 1988]. The climate may have also played a role in this orogenic process, due to complex feedback between sea-land distribution, orography, and monsoon [*Molnar and England*, 1990]. In all cases, the elevations with respect to time are not well constrained, and for instance, the period when the Tibetan plateau reached its present-day elevation is dated between the middle Miocene [*Turner et al.*, 1993; *Coleman and Hodges*, 1995] and the late Miocene [*Harrison et al.*, 1992].

We have first assumed (Figure 1a) that a mountain range of moderate elevation (2500 m) was located along the Yarlung-Zangbo suture (boundary of the Indian-Eurasian blocks) at 30 Ma (Oligocene reconstruction) and rejuvenated the Gangdese batholith [*Yin et al.*, 1994]. The rest of the future Tibetan plateau remained a low land (about 500 m), with probably smooth relief as confirmed by paleodata suggesting the presence of subtropical flora, found for example in the Lumpola basin, central Tibet [*Ren*, 1981]. A rapid pulse of uplift of the Gangdese batholith [*Copeland et al.*, 1987; *Richter et al.*, 1991] and High Himalayas crystalline chain [see *Amano and Taira*, 1992; *Harrison et al.*, 1992; *Hodges et al.*, 1992; *Yin et al.*, 1994 for reviews] lead to an important thrusting along the Main Central Thrust (MCT) during the lower Miocene (17 Ma). A second important uplift phase of the High Himalayas then occurred during the middle-late Miocene (around 10 Ma) [*Harrison et al.*, 1992], with the creation of a new thrust zone, the Main Boundary Thrust (MBT). We chose a mean elevation value of 4000 m in our 10 Ma reconstruction that is in agreement with the conclusion of *France-Lanord et al.* [1993]. We have used the work of *Tapponnier et al.* [1990] and *Meyer et al.* [1998] to constrain the elevation of the Tibetan plateau. The topography is characterized by a progressive northward shift of the areas affected: the elevation of the southern Tibetan plateau reaches some 3000 m as the result of continental subduction within the ancient Bangong suture. The elevation to the north, close to the Jinsha region, has a lower elevation of some 1000 m. This situation corresponds to a progressive buildup of the plateau at its northern edge.

In North America, the mountain belt existed since at least the middle Cretaceous. Nevertheless, the elevation of this chain is much higher today than it was during the last 30 Myr [*Ruddiman et al.*, 1997b]. We prescribe for this mountain belt, a low mean altitude (less than 1000 m) at the Oligocene [*Bird*, 1988] (Figure 1a), remnant of the Laramide orogeny (75-45 Ma). The tectonic evolution of the western continental part was driven by the subduction of the Pacific plates during the Cenozoic [*Oldow et al.*, 1989]. The segmentation of this subduction zone has induced a transition from compressive to extensive regimes in western America. This transition led to the opening of grabens in the Basin and Range areas and to its gravitational collapse [*Stewart*, 1977]. Consequently, this structure was higher during the Oligocene period than at present, but due to its surface and to the interpolation on the grid model, this feature does not appear clearly in our reconstruction. The uplift of the Rocky Mountain range and of the Colorado plateau occurred after 24 Ma, as deduced from paleodrainage systems suggesting an opposite flow direction since the Miocene [*Scott*, 1977]. We have assigned a mean height close to 1500 m for the Miocene topography (Figure 1b).

Since the late Oligocene, the increased subduction rate of the Nazca oceanic plate has driven the formation of the Andes, along the Pacific Coast [*Sébrier et al.*, 1988]. Nonetheless, this uplift is not homogeneous over the full range length and also not continuous through time [*Hoorn et al.*, 1995]. Compressive and extensive phases alternated within the central Andes during the late Cenozoic. A linear uplift is used in our models to build up the South American topography. The Oligocene topography is characterized by a low orography (less than 1000 m) with a discontinuous mountain range along the Pacific Ocean (Figure 1a). At 10 Ma (Figure 1b), we affect a continuous range with a half altitude with respect to the present day. The Andes is not, at any rate, well depicted on our map because of its limited longitudinal extent with respect to the model resolution (Figure 1c).

Eastern African regions have experienced several phases of uplift during the late Tertiary [*Baker*, 1971; *Partridge*, 1997]. We kept the relief nearly unchanged with respect to the present day (Figures 1a and 1b). This mountain range does not exhibit high elevation, with the exception of the Ethiopian traps dated at 30 Ma [*Hofmann et al.*, 1997].

Since the early Cenozoic, Australia has drifted northward with the Indian plate. During the Oligocene period, the Australian craton was greatly emerged [*Lorenz et al.*, 1993]. It also underwent uplift in its southeastern part, which is not represented because of the low resolution of our model.

2.4. North and South Glaciations: Antarctica and Greenland

The onset of Antarctic ice sheet formation [*Ehrmann and Mackensen*, 1992] is linked to the intensification of the circum-Antarctic circulation [*Kennett et al.*, 1975] due to the opening of

the Drake Passage during the Oligocene [*Diester-Haass and Zahn*, 1996; *Rack*, 1993]. Since this epoch, this ice sheet underwent important fluctuations, although it never entirely disappeared. The progressive buildup of the ice sheet has influenced the global climate, especially the pole-equator gradient in the southern hemisphere. Because this study concerns the impact of paleogeography on climate changes, we have considered that the Antarctic ice sheet had already built up since the Oligocene.

In the northern hemisphere, the glaciation started at 3 Ma. However, evidence exists for seasonal sea ice in the Arctic Ocean in the early Miocene [*Zubakov and Borzenkova*, 1990]. Glaciation of the Greenland continent occurred during the end of the Pliocene [*Shackleton and Opdyke*, 1977]. Consequently, we removed the Greenland ice sheet in both simulations (10 and 30 Ma). The Greenland orography (Figures 1a and 1b) has been adjusted accounting for the isostatic response due to its absence of ice sheet.

3. Model and Run Descriptions

3.1. The LMD Model

To perform our numerical experiments, we used the Laboratoire de Météorologie Dynamique (LMD) version 5.3 AGCM [*Harzallah and Sadourny*, 1995]. This three-dimensional (3-D) model solves the dynamic and thermodynamic equations, continuity equations for mass, energy, and water vapor transport using a finite element scheme. This is a grid-point model with a standard resolution corresponding to 64 points regularly spaced in longitude, 50 points distributed in sine of latitude. The surface of the cells is equal and corresponds to 400 by 400 km^2 at midlatitudes and reaches a finer latitudinal resolution at low latitudes (250 km at 30°N and 220 km at the equator). The model has 11 vertical levels in normalized pressure coordinates; four lower levels are devoted to the boundary layer, four for the rest of the troposphere, and three for the stratosphere up to 30 km. It includes a full seasonal cycle but no diurnal cycle for insolation. The radiative schemes for solar and infrared radiation are adapted from *Fouquart and Bonnel* [1980] and *Morcrette* [1991], respectively. The AGCM includes a soil model, accounting for the impact of a prescribed vegetation [*Ducoudré et al.*, 1994]. Each simulation lasts 16 years, and averages of parameters are made on the last 15 years to represent the climatic equilibrium reached by the model.

3.2. Set of Simulations and Boundary Conditions

Three experiments were performed (Table 1) including a simulation for the present day (PD) (which is our control experiment (Exp0)), a simulation of the middle late Miocene (10 Ma, Exp1) and finally, a simulation of the Oligocene (30 Ma, Exp2). For each period, the climate model requires a set of prescribed boundary conditions. This set includes the global paleogeographic reconstruction (land-sea distribution and orography) as previously described. The other prescribed boundary conditions are SST, vegetation, CO_2 atmospheric content, and orbital parameters. For the SSTs, we attributed present-day values when possible. When continental grid points become oceanic grid points due to plate motions, we assign the value of the closest grid point of an equivalent nature at the same latitude. For example, we use the present-day SSTs of the Caspian and Black Seas for the Paratethys Sea. This procedure has been preferred to an easier one consisting in using PD zonal averaged value for SST, inducing a strongly zonal atmospheric circulation and thus, cooling deeply the inner continent [*Ramstein et al.*, 1997b]. Recent climate investigations [*Dong et al.*, 1997; *Kutzbach et al.*, 1993] use an AGCM coupled to a slab ocean but prescribe the meridional oceanic heat fluxes. We have also performed such experiments with the LMD AGCM at lower resolution coupled to a slab ocean (LMD4ter, 48x36 grid points) to quantify the influence of changes in thermal response of the ocean. The conclusions on the Asian monsoon and the Eurasian climate remain similar to those obtained with an AGCM not coupled to a slab ocean [*Ramstein et al.*, 1997a]. Moreover, as discussed in section 1, there is no drastic variation of the global oceanic circulation since the Oligocene.

According the modeling curve of *Berner* [1992], the CO_2 atmospheric content decreased by half from the Oligocene to the present day. This is in agreement with atmospheric CO_2 concentration for the past 10 Myr deduced from stomata densities of fossil leaves [*Van der Burgh et al.*, 1993], suggesting fluctuations between 280 ppm and 370 ppm. However, we chose to keep it unchanged in order to focus only on the impact of paleogeographic changes. Thus we specified PD value (345 ppm) in all our simulations. We also use the PD values for Earth's orbital parameters. Finally, for the soil-atmosphere interaction, the LMD5.3 AGCM includes an interface scheme [*Ducoudré et al.*, 1994] that accounts for the influence on climate of a prescribed vegetation. Vegetation changes are able to modify the climate locally [*De Noblet et al.*, 1996; *Otto-Bliesner and Upchurch*, 1997]. We have, however, kept the present-day vegetation distribution, except for the "newly" emerged land points, where we have used the nearest neighbor method as already described for the SSTs.

Table 1a. The Set of Realistic Experiments

Experiment	Age, Ma	Comparisons	Impact
0	PD	Exp0-Exp1	paleogeography
1	10	Exp1-Exp2	paleogeography
2	30		

Table 1b. The Set of Sensitivity Experiments

Experiment	Age, Ma	Paleogeographic Changes	Comparisons	Impact
3	PD	reduced Tibetan plateau elevation	Exp0-Exp3	Tibetan uplift at PD
4	10	reduced Tibetan plateau elevation	Exp1-Exp4	Tibetan plateau at 10 Ma
5	10	reduced Paratethys Sea	Exp5-Exp1	partial Paratethys retreat at 10 Ma
6	30	reduced Paratethys Sea	Exp6-Exp2	partial Paratethys retreat at 30 Ma
7	30	no Paratethys Sea	Exp7-Exp2	full Paratethys retreat at 30 Ma

3.3. Ability of the LMD AGCM to Simulate the Present-Day Monsoon

The LMD5.3 AGCM reproduces the main features of the Asian and African monsoons [*De Noblet et al.*, 1996]. Asian precipitation is relatively faithfully simulated by the AGCM, with the exception of an overestimate over the eastern Himalayas and southern China. The rainfall is directly linked to both the westerly and the Somali jet, which bring moisture from the Indian Ocean. The wind intensity is relatively well simulated, but the westerly does not converge enough toward India and induces a too dry climate over northern India. This is a common drawback of several AGCMs. In Africa, rather good agreement is obtained for the locations of heavy rainfall, greater than 5 mm/d (Guinea coast, Nigeria). Strong rainfall values simulated over the Ethiopian highlands are excessive. On the other hand, the light precipitation, weaker than 2 mm/d, simulated by the LMD AGCM over the southern part of Sahara is unrealistic. Although most of the African monsoon precipitation is correctly represented, comparison with European Centre for Medium-Range Weather Forecasts (ECMWF) analyses clearly shows an overestimation of the simulated wind intensity. This is again a common flaw to many AGCMs [*World Climate Research Program*, 1993]. Although slight discrepancies exist, the LMD AGCM is able to simulate most of the characteristics of the present-day African and Asian monsoons both in spatial rainfall distribution and duration, realistically enough to be used for paleoclimatic purposes.

4. Simulated Asian Monsoon Since 30 Myr

4.1. Evolution of Temperature and Precipitation Since 30 Myr

The main cause of the Asian monsoon is in the thermal gradient between the continent and the Indian Ocean. In the Oligocene simulation, the Paratethys Sea in Eurasia restricts heating of the inner continent. The progressive retreat of the Paratethys enhances the continental climate over central Eurasia [*Ramstein et al.*, 1997a], characterized by a winter cooling (-10°C) and a summer warming (+8°C) from Oligocene to PD, increasing the land-ocean temperature gradient. We also observe in this area that the summer warming is stronger between the PD and 10 Ma (Plate 1a) than between 10 Ma and 30 Ma (Plate 1b) whereas the cooling presents the opposites pattern (Plates 1c and 1d). However, the amplitude of these changes relies partially on SST values that we prescribed for the Paratethys Sea at 30 Ma. The uplifts of the Tibetan plateau and Himalayas induce an annual cooling over these areas consistent with a 6°C/km lapse rate. The winter cooling simulated over the Tibetan plateau and over Eurasia is partly due to the albedo feedback superimposed to the impact of the uplift. Focusing on the summer period at midlatitudes, we suggest that the strong warming between 10 Ma and PD results from both the final retreat of the Paratethys Sea and the uplift of the Tibetan plateau [*Ramstein et al.*, 1997a]. This climatic change over central Asia is marked by an atmospheric circulation diverted southward due to the Tibetan uplift [*Hahn and Manabe*, 1975; *Kutzbach et al.*, 1993].

The atmospheric circulation changes and the Paratethys shrinkage induce a drying of this area (Figures 2a and 2b) and a weakening of cloudiness which acts as a positive feedback on the summer temperature. These climatic changes are confirmed by vegetation changes observed in Asia. The caduceus and subtropical vegetation are replaced by conifers in Siberia and by steppe in central Asia during the Miocene [*Traverse*, 1982; *Zubakov and Borzenkova*, 1990].

The strengthening of the land-sea temperature gradient increases the monsoon advection and thus enhances precipitation from Oligocene to PD [*Ramstein et al.*, 1997a]. Figure 2 shows the summer (June-July-August) precipitation distribution for each period. The simulated monsoon rainfall in the Oligocene experiment (Exp2) (Figure 2a) is mainly located over Indochina, whereas the intensity of precipitation is rather weak over the Himalayas. For the middle Miocene (Exp1) (Figure 2b), the rainfall is enhanced over the Himalayas but reduced over Indochina. These trends are further enhanced in the control experiment (Exp 0) (Figure 2c), with increased precipitation over India, over the Himalayas, and on the eastern margin of the Tibetan plateau. These changes are statistically significant at the 95% level in a T-test. We compute the mean summer precipitation change over Indochina (90°E-110°E and 0°-25°N). The mean summer precipitation reaches 19 mm/d during the Oligocene (Exp2), only 15.2 mm/day (-3.8 mm/d) for the middle-Miocene (Exp1), and 11.3 mm/day (-3.9 mm/d) for PD (Exp0). This decrease is mainly explained by a weakening of the heavy rainfall events (greater than 10 mm/d). The change in seasonal contrast is rather weak. The decrease of the monsoon precipitation over Indochina is not seen in data which show a relative climatic stability [*Ducrocq et al.*, 1994]. We suggest that despite reduced precipitation over Indochina, the monsoon climate prevailed since the Oligocene. The decrease in precipitation over Indochina does not agree with the abrupt increase of the terrigeneous accumulation rate filling the adjacent basins [*Métivier*, 1996]. This sedimentary evolution is probably more influenced by tectonic activity and sea level fluctuations than by climatic changes. Based on paleoenvironment changes in lakes, *Chenggao and Renaut* [1994] suggested that a monsoon circulation existed during most of the Cenozoic period in south China and migrated northward since 30 Ma. Their idea is also supported by changes in vegetation [*Leopold et al.*, 1992; *Wang*, 1994]. The progressive northward drift of the monsoon is clearly simulated in our experiments and is directly induced by the evolution in elevation of the eastern margin of the Tibetan plateau which strengthens the advection over this area.

Figure 2 also shows an important feature: the progressive separation between monsoon rainfall and the annual belt of equatorial precipitation over southern India (5°N-15°N; 80°E) due to the northward drift of India. A single precipitation center was simulated over southern India at 30 Ma (Figure 2a) whereas we observe two areas of precipitation at PD (Figure 2a), one over southern India (15°N, 80°E) and the other over the Equator. This latter is less sensitive to monsoon changes. The climatic evolution in southern India is consistent with paleodata which suggest the decrease of tropical forests and the emergence of savanna [*Traverse*, 1982]. The shift from C3 to C4 photosynthetic pathway during the late Miocene [*Quade et al.*, 1989; *Cerling*, 1997, *Cerling et al.*, 1997] may also explain this vegetation change.

To go one step further, we have analyzed more accurately the precipitation changes over the Himalayas (84°E-106°E and 25°N-30°N). This area includes both the mountain range and the foreland basin. We then compare our climatic parameters with the evolution of the Bengal fan sedimentation. It is indeed generally thought that the terrigeneous sediments of this area find their main source in the erosion processes of the Himalayas. This interpretation is supported by their isotopic signature similar with

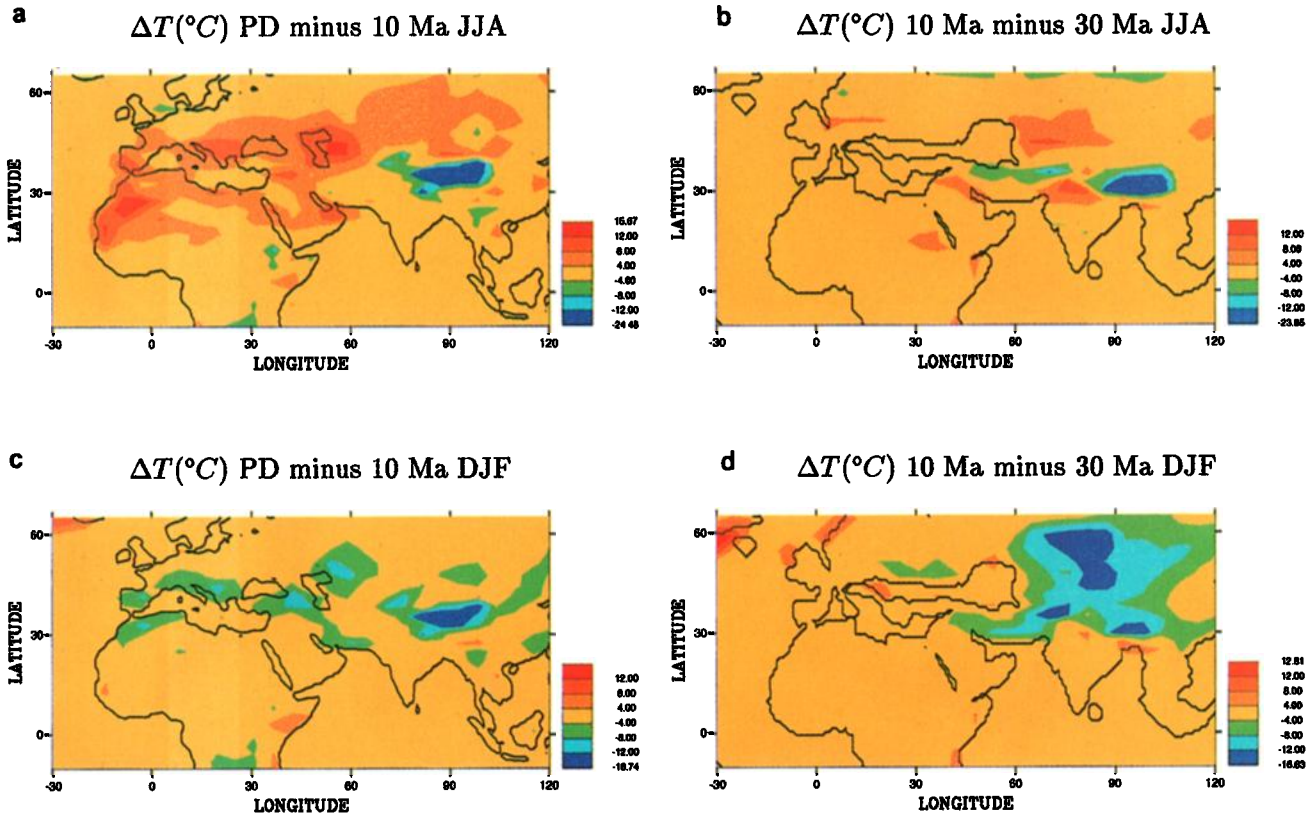

Plate 1. Mean temperature differences (°C) over Eurasia : (a) PD (Exp0) - 10 Ma (Exp1) in summer, (b) 10 Ma (Exp1) - 30 Ma (Exp2) in summer, (c) PD (Exp0) - 10 Ma (Exp1) in winter, and (d) 10 Ma (Exp1) - 30 Ma (Exp2) in winter. Cooling is in green and blue, warming is in orange and red, and no change is yellow.

those of the High Himalayan crystalline series [*France-Lanord et al.*, 1993; *Derry and France-Lanord*, 1997].

Accounting for the variability of the signal, the summer precipitation (Figure 3a) increases quite linearly from the Oligocene (5.8 mm/d) to the middle-late Miocene (10.2 mm/d) to the PD (14.2 mm/d). However, the strengthening of mean summer precipitation is twice as strong in the past 10 Myr (+0.4 mm/d/Myr) as from 30 Ma to 10 Ma (0.22 mm/d/Myr). The temporal distribution of rainy events may give further information. We only present the evolution of the number of days with the strongest rains in summer (Figure 3b) which are responsible for strong erosion processes [*Kutzbach et al.*, 1997]. The number of days marked by intense rains clearly increases with time, reaching +31% (days/month) between 30 Ma and 10 Ma and 50% (days/month) between 10 Ma and PD. The increase is also more conspicuous in the past 10 Myr (+0.42 day/Myr) than between 30 Ma to 10 Ma (+0.13 day/Myr). This evolution is associated with an increase in summer rainfall concentration representing 33% of the annual value at 30 Ma, 43% at 10 Ma, and 64% today (Figure 3c). The last 10 Myr are characterized by an intensification in seasonality which is 4 times as strong as between 30 Ma and 10 Ma. These results point out an intensification of the monsoon precipitation and also a significant strengthening of the seasonal contrast which may drive peak discharges of sediment [*Summerfield*, 1991]. We then compute the annual mean precipitation over the Himalayas (Figure 3d). Previous studies [*Kutzbach et al.*, 1989; *Prell and Kutzbach*, 1992; *Kutzbach et al.*, 1993; *Ramstein et al.*, 1997a] only focused on the summer monsoon because winter monsoon carries little moisture [*Hastenrath*, 1985]. The mean annual precipitation increases by +1.52 mm/d from 30 Ma to 10 Ma and decreases by 0.38 mm/d from 10 Ma to PD.

The sedimentary evolution of the Bengal fan remains complex. On one hand, there is a clear increase of the mean sediment accumulation rate integrated over the entire basin [*Métivier*, 1996] starting between 10 and 5 Ma. This study is mainly based on proximal deposits. One the other hand, the analysis of three very well dated cores from the Ocean Drilling Program (ODP) leg 116 and 117 [*France-Lanord et al.*, 1993] show a sudden diminution of the accumulation rate from 7 Ma (late Miocene) to 1 Ma. Our simulations do not display any abrupt changes in the summer monsoon intensity from Oligocene to PD. This characteristic is also observed by other sensitivity studies using a gradual mountain uplift [*Kutzbach et al.*, 1989; *Valdes*, 1997]. The increases of both seasonal contrast which may have contributed to the C3/C4 vegetation shift in the Siwaliks [*Quade et al.*, 1989; *France-Lanord and Derry*, 1994], and strong rainy event days agree well with the brutal increase of the mean accumulation rate integrated over the entire basin. Conversely, they do not fit the sedimentation slow down in the distal Bengal fan. This last signal appears more similar to the evolution of our simulated mean annual precipitation. The effect of our strong increase of seasonality is to favor rapid transport of the eroded products toward the Ocean and a major accumulation in proximal zones is likely, while the ODP leg corresponds to a distal position, receiving thus the finest terrigeneous fraction. We, however, recall that the relationships between monsoon and orogeny are very complex [*Molnar et al.*, 1993; *Rea*, 1992], and

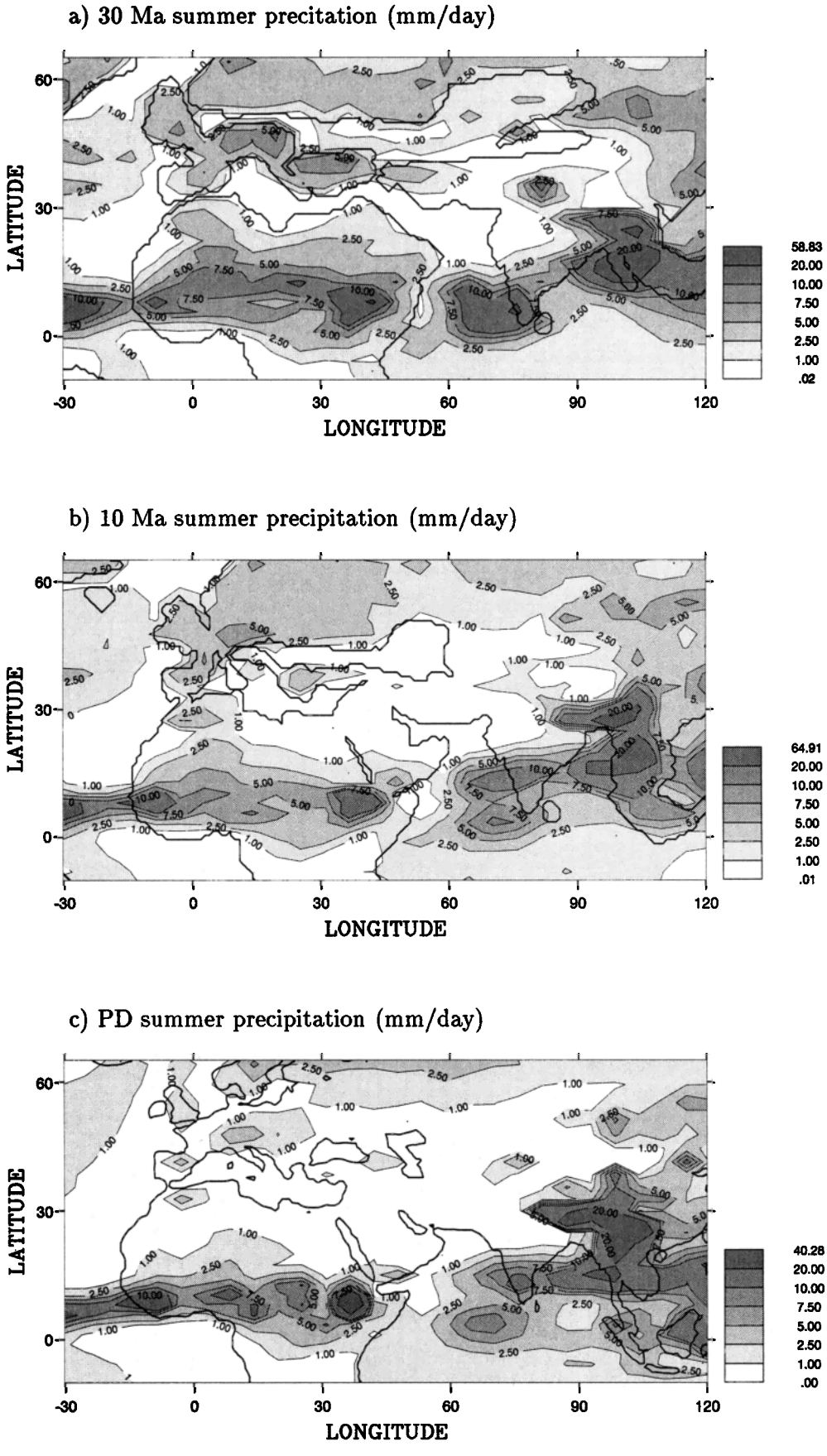

Figure 2. Mean summer precipitation (mm/d) over Eurasia at (a) 30 Ma (Exp2), (b) 10 Ma (Exp1), and (c) PD (Exp0). Isolines are plotted for 1, 2.5, 5, 7.5, 10, 20 mm/d. White represents rainfall lower than 1 mm/d (arid area), and the dark gray scale represents the wettest areas (>10 mm/d).

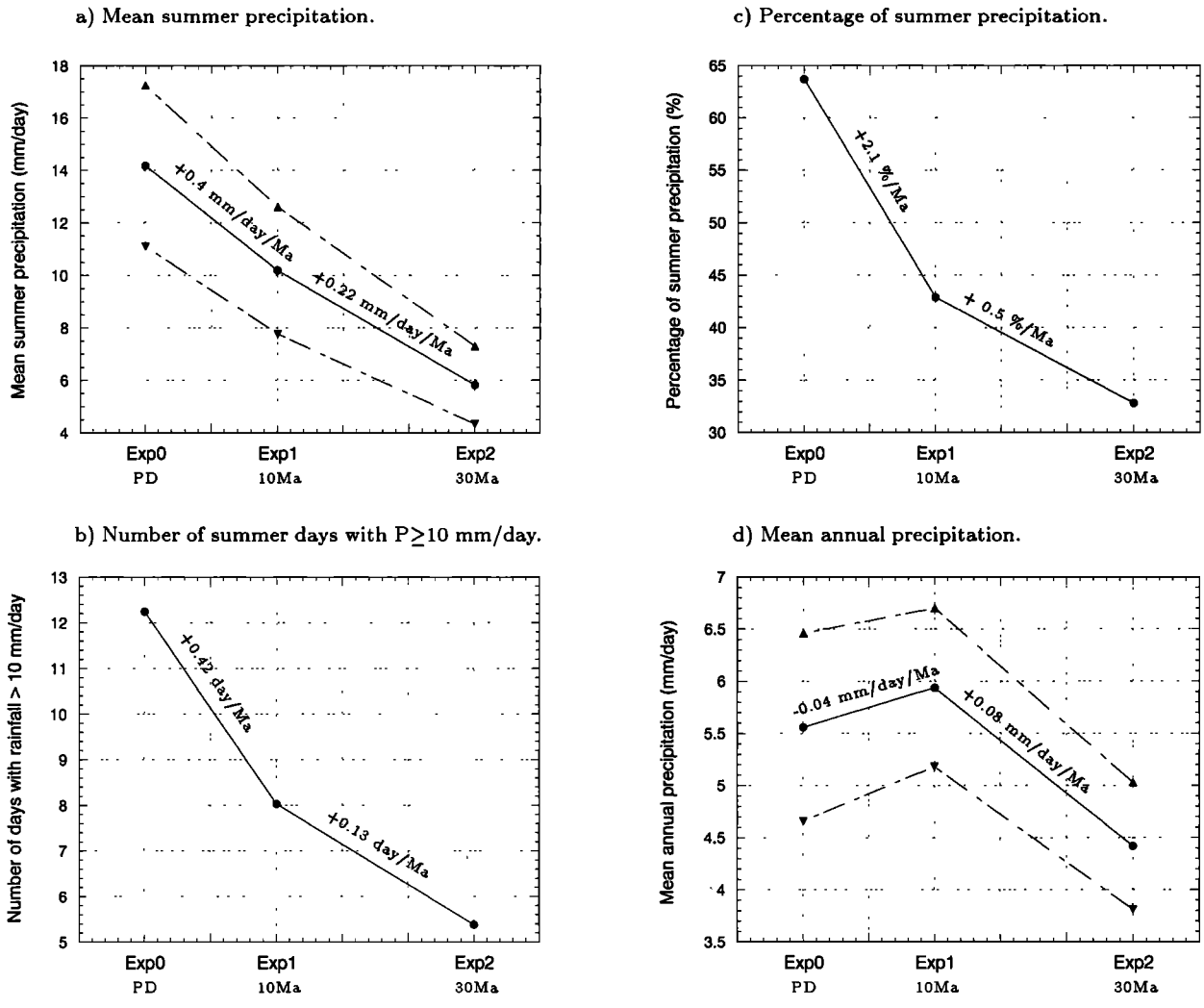

Figure 3. Precipitation evolution averaged over the Himalayas and the foreland at PD (Exp0), 10 Ma (Exp1), and 30 Ma (Exp2). (a) Mean summer precipitation (mm/d), (b) number of days in summer precipitation stronger than 10 mm/d (days/month), (c) percentage of mean summer precipitation relative to mean annual precipitation, and (d) mean annual precipitation (mm/d). The continuous line indicates the mean value; the dashed lines represent the signal accounting for the variability. The values on each plot indicate the mean amplitude of the changes per million years between 10 Ma and PD and between 30 Ma and 10 Ma.

it seems difficult to separate in the sedimentary record, the parts linked to an enhancement of erosion resulting from increased precipitation from those resulting from tectonic activity.

4.2. Evolution of Atmospheric Dynamics

The precipitation evolution over the Himalayas and Indochina since the Oligocene exhibits opposite features. Although we simulate a decrease of precipitation over Indochina, a wet summer monsoon associated with an important seasonal contrast is maintained since 30 Ma. We point out a northwestward drift of the whole monsoon system. To explain such a drift, we will analyze the evolution of the large-scale atmospheric circulation using sea-level pressure and wind fields. A deep low-pressure cell induced by the warming of the continent characterizes the monsoon. The 1000 hPa isoline (indicated by the 0 hPa isoline on Figure 4) is used to describe the low-pressure cell. For the Oligocene experiment (Figure 4a), the low-pressure cell is reduced. Its extent is limited to India and southern China because, on the one hand, the Paratethys high-pressure cell limits its northwestward extent and, on the other hand, the Tethys seaway separates the Asian thermal trough from the one located over Arabia. For the middle Miocene experiment (Figure 4b), the Asian thermal trough expands only from western India to China. Today, the Asian low-pressure cell spreads from northern China to Arabia and is centered over northwestern India (Figure 4c). The low-pressure cell shifts progressively northwestward from southeastern Asia toward the Middle East. The center of this system follows the same trends and shifts northwestward over northern India. The changes in low-pressure cell result from changes in land-sea distribution and from the orographic evolution. Among the paleogeographic changes, the Paratethys Sea above which a high-pressure cell is located, controls strongly the stretching of the Asian trough, whereas the minimum pressure is driven by the release of latent heat over the flank of a mountain range.

The 850 hPa winds also reflect the changes in atmospheric circulation (Figure 4). The strong westerly located over Bengal

a) 30 Ma sea level pressure (hPa) and wind at 850 hPa (m/s) in summer

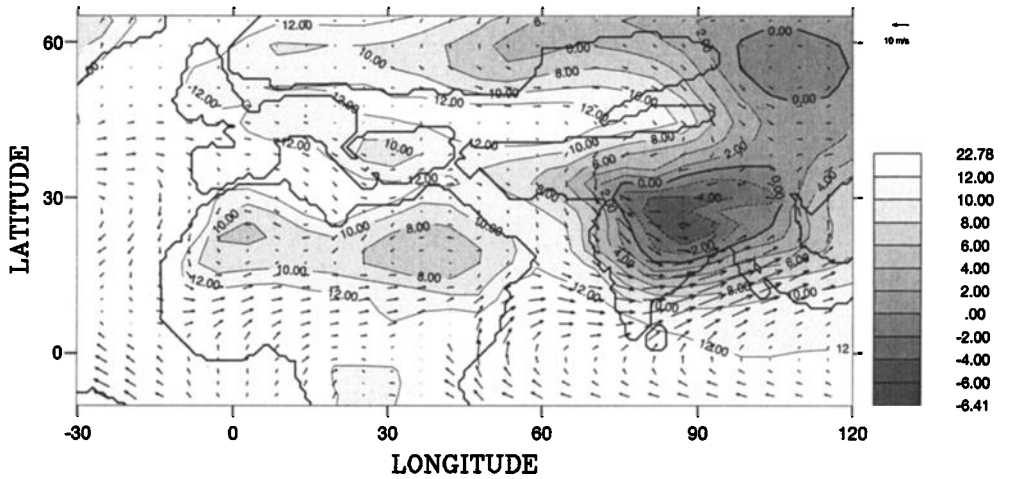

b) 10 Ma sea level pressure (hPa) and wind at 850 hPa (m/s) in summer

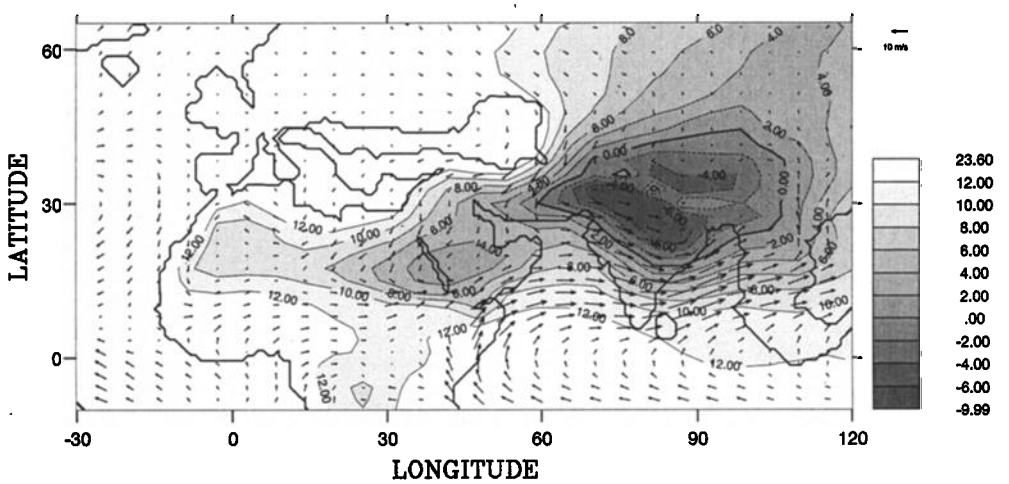

c) PD sea level pressure (hPa) and wind at 850 hPa (m/s) in summer

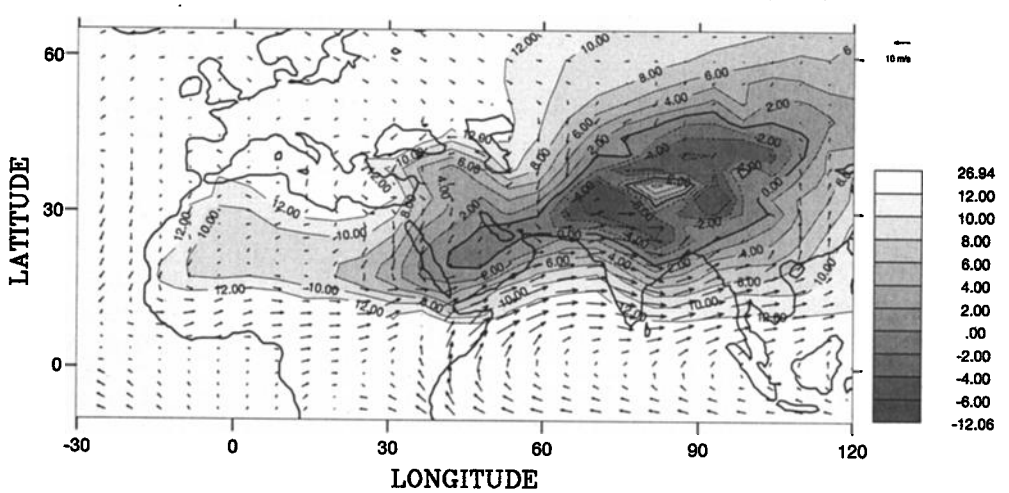

Figure 4. Mean sea level pressure (minus 1000 hPa) and wind field at 850 hPa in summer at (a) 30 Ma (Exp2), (b) 10 Ma (Exp1), and (c) PD (Exp0). The pressure interval is 2 hPa. Thick line represents the 1000 hPa pressure (noted 0 hPa on the figure). An adjustment factor has been added to the Oligocene and middle late Miocene sea level pressure to compensate for the difference in mean global elevation. This factor corresponds to the mean annual difference of pressure averaged over the globe between the experiments at 10 Ma or at 30 Ma and the present day. Grey scale indicates the low-pressure cell; white areas represent sea level pressure greater than 12 hPa. Vectors represent the wind, both in direction and amplitude.

Bay, which produces heavy precipitation over Indochina during the Oligocene (Figure 4a), slows down progressively. The low-pressure cell evolution since 30 Ma is accompanied by an intensification of wind over the Arabian Sea (Figure 4c) and by local feedback due to convective motion. An increase of the moisture convergence toward the Himalayas results from this evolution and thus explains the enhancement of precipitation over the Himalayas.

So far, we have analyzed the monsoon circulation at low atmospheric levels. We show now that the paleogeographic changes also contribute to changes in the upper atmospheric circulation. We investigated the evolution of the monsoon in altitude-latitude plots (Figure 5) averaged between 75°E and 90°E crossing the Indian subcontinent, southwestern Bengal Bay, the Himalayas, the Tibetan plateau, and northward until western Siberia, to depict the major changes in vertical wind and atmospheric water vapor content (not shown). At 30 Ma, the atmospheric rising motion over the Himalayas is weak and occurs on both sides of the Himalayas (Figure 5a). The rising air mass over its northern flank reflects the release of latent heat brought from the Paratethys Sea and may explain the presence of subtropical vegetation in Tibet in 30 Ma [*Ren*, 1981]. Moreover, the vapor content which is relatively uniform over both sides of the Himalayas in the Oligocene experiment, increases progressively above its southern flank and northern India in relation to the increase of moisture convergence and decreases over the northern flank. Conversely, water vapor decreases over the northern flank, on the Tibetan plateau, and over Siberia because of the changes in atmospheric circulation and the retreat of the Paratethys that previously provided a large source of moisture. In the 10 Ma experiment (Figure 5b), the ascending motion over the southern Himalayas is strongly strengthened. In the PD simulation (Figure 5c), two areas of rising air masses located above India (15°N) and the southern flank of the Himalayas (30°N) are simulated. They reflect the release of latent heat by precipitation. Large vertical motion affects the upper troposphere (300 hPa) over the Himalayas, inducing an important advection.

4.3. Moisture Advection Over the Arabian Sea

The Somali jet blowing over the Indian Ocean and Arabian Sea carries moisture toward southern Asia (Figure 4c). The Arabian Sea contributes more than half of the atmospheric moisture transported over the continent in the model. Thus the location of the strongest winds over the Arabian Sea and their moisture content are of critical importance in the evolution of the Asian monsoon.

Over the Arabian Sea, the limit of confluence between the northwesterlies and the southwesterlies defines the Inter-Tropical Convergence Zone (i.e., ITCZ). The position of this confluence provides further information on monsoon dynamics. We estimate the latitude of confluence using the meridional wind component averaged between 55°E and 70°E (Figure 6). Negative values connote northwesterly (blowing from the central Eurasia), whereas positive values imply southwesterly (blowing from the Indian Ocean). To complete this analysis, we have calculated the mean amount of latent heat carried in the boundary layer (the first fourth lower atmospheric layers in the LMD AGCM) in two areas located over the Arabian Sea. These areas stretch from 55°E to 70°E and from the Equator to 32°N. The boundary between these zones is defined by the ITCZ latitude deduced from Figure 6. During the summer monsoon, the major part of the moisture crosses both areas. The latent heat flux crossing the Equator between southern India (75°E) and Indochina (100°E) affects southeastern Asia. In the 30 Ma experiment, the southwesterlies/northwesterlies convergence is located at 11°5N

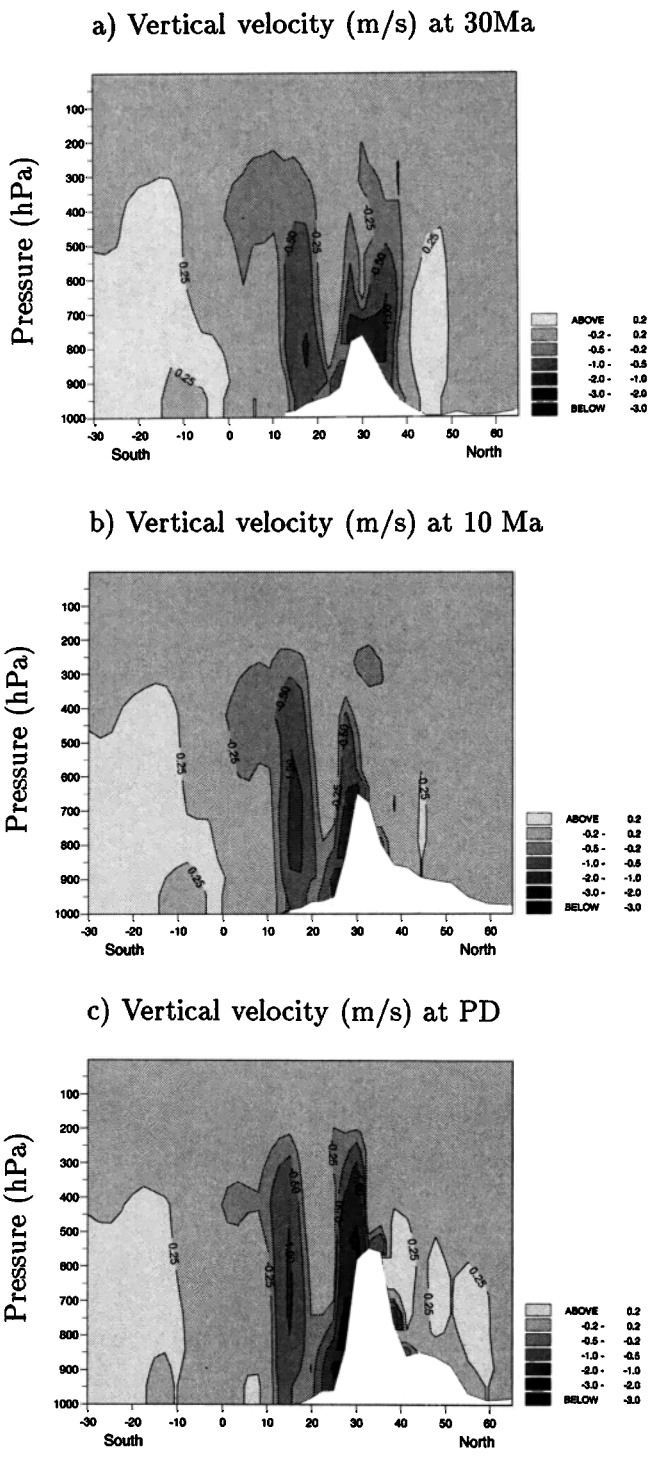

Figure 5. Mean vertical velocity in summer averaged in longitude between 80°E and 95°E at (a) 30 Ma (Exp2), (b) 10 Ma (Exp1), and (c) PD (Exp0). The vertical scale is pressure (hPa) and represents the atmosphere from sea level to 30 km height. Light gray areas are attributed to subsidence (positive values), dark gray indicates ascending motion (negative values), and white represents the orographic contour (Himalayas and Tibetan plateau).

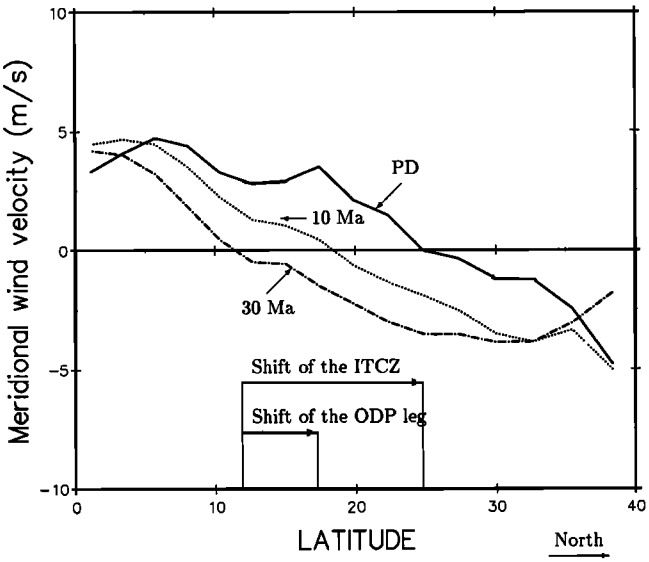

Figure 6. Meridional wind velocity (m/s) in summer averaged in a band stretching over the Arabian Sea (45°E-65°E). Values equal to 0 m/s define the latitude of ITCZ. The ITCZ is located at 11°5N at 30 Ma (Exp2), 18°N at 10 Ma (Exp1), and 25°N at PD (Exp0).

(Figure 4a). The southwesterlies advect about 63% of the total latent heat flux over the Arabian Sea (37% for the northwesterlies). The closure of the Tethys and Paratethys as well as the uplift modify the configuration of the monsoon trough (Figure 4b), shifting the ITCZ northward up to 18°N (Figure 6). The part of the latent heat transport carried by the northwesterlies reaches 12%, whereas the southwesterlies bring 88% of the moisture. The final Paratethys retreat and the end of Tibetan uplift lead to the westward extent of the monsoon trough (Figure 4c). The PD confluence migrates farther north to 25°N (Figure 6). The part of the total latent heat advected by the southwesterlies reaches 97% versus only 3% for the northwesterlies. Superimposed to this redistribution of the latent heat transport, the southwesterlies increase by 20% between 10 Ma and PD (-65% for the northwesterlies). The configuration of the monsoon trough implies a redistribution of the advected fluxes.

The difference of the mean sea level pressure between central Asia (Paratethys high) and northern India (monsoon trough) reveals that the middle Miocene experiment has the strongest gradient (Figure 4b). For the Oligocene experiment (Exp2), the eastward location of the high-pressure advects moisture toward the northwestern flank of the relief (Figure 4a). The shifted high-pressure cell over central Asia at 10 Ma brings more moisture over India and the southern flank of the Himalayas than over the northern flank.

The northward motion of the ITCZ over the Arabian Sea may also be compared to the upwelling evolution which reflects the summer monsoon wind field [*Kroon et al.*, 1991; *Nigrini and Caulet*, 1992]. The raising of cold and nutrient-rich water masses led to the development of planktonic foraminifera (*Globigerina bulloides*). This population is thus an indicator of the intensity of monsoon winds [*Prell et al.*, 1990; *Curry et al.*, 1992]. At geologic timescales, the sediment core presents a fossil population which is a good recorder of the past monsoon variability [*Kroon et al.*, 1991; *Prell and Kutzbach*, 1992; *Emeis et al.*, 1995]. The abrupt increase of foraminifera recorded in the sediments of the Arabian Sea (site ODP 722, Owen ridge) occurred during the late Miocene (7-8 Ma). It has been related to an abrupt development of the Asian monsoon onset and may be considered as the most relevant evidence since these data only depend on the southwesterlies intensity over the Arabian Sea [*Kroon et al.*, 1991; *Nigrini and Caulet*, 1992; *Prell and Kutzbach*, 1992]. However, *Sirocko* [1991] showed that fluctuations in upwelling intensity depend on the position of the ITCZ during the Quaternary and reflect the glacial/interglacial cycles. During the interglacial epochs, since the Asian monsoon and thus the southerlies are stronger, setting the ITCZ in a northern position over the Arabian Sea, upwellings are clearly recorded in the sediment core. Conversely, during the glacial periods, the northwesterlies over the Arabian Sea (characterized by an increase of Arabian dust dispersal) are intensified, shifting the ITCZ southward and inhibiting upwelling.

We suggest that this mechanism explains the increase of the upwelling intensity during the late Miocene. The increase of upwelling deduced from sediment core (ODP 722) does record the northward shift of the monsoon wind system and the ITCZ during the Cenozoic. Accounting for the Arabia northward motion of some 6° at the latitude of the drilling site, the sediment core was located from 30 Ma to 10 Ma under the ITCZ. The monsoon wind system is located southward during both periods. The shift of the monsoon system may explain the absence of upwelling development detected in the sediment core until the late Miocene. Besides the location of the drilling site with respect to the southwesterlies, we also observe a weakening of these winds over the Arabian Sea. Weak winds reduce the Ekman current and may inhibit upwelling. Finally, the opened Tethys seaway and a surface current may also restrain upwelling despite weak exchange between the Atlantic and Indian Oceans. These climatic, paleogeographic, and oceanic factors may interfere in the development of endemic upwelling species.

5. Impact of Plateau Uplift and Paratethys Shrinkage

Because the Tibetan uplift and the Paratethys shrinkage may have a strong impact on the summer Asian monsoon since 30 Ma, we have performed a set of sensitivity experiments (Table 1b and Figure 7) to quantify their respective actions. The AGCM is forced with the paleogeographic reconstruction at PD, 10 Ma, and 30 Ma, in which we remove a part of the Paratethys Sea or reduce the Tibetan plateau height. Because the AGCM computes an atmospheric response in equilibrium with the prescribed boundary conditions, the difference between the "realistic" and sensitivity experiments represents the impact of each forcing factor on the climate. Thus, to quantify the impact on a climatic parameter (X) of each geologic event independently, we have calculated the difference of values obtained in the sensitivity experiment (X_s) and in the realistic experiment (X_r) for the same geologic period. This difference $(X_s\text{-}X_r)_{age}$ is compared to the differences between two "realistic" experiments $(X_r)_{age1}\text{-}(X_r)_{age2}$.

To investigate the role of the Tibetan plateau uplift on the strengthening of the monsoon, we have performed two runs (Table 1b). Contrary to previous studies [*Kutzbach et al.*, 1989, 1993], we have only modified the elevation of the Tibetan plateau and we have kept unchanged the Himalayas. The differentiation between the Himalayas and the Tibetan plateau is due to their distinct geologic evolutions in time [*Tapponnier et*

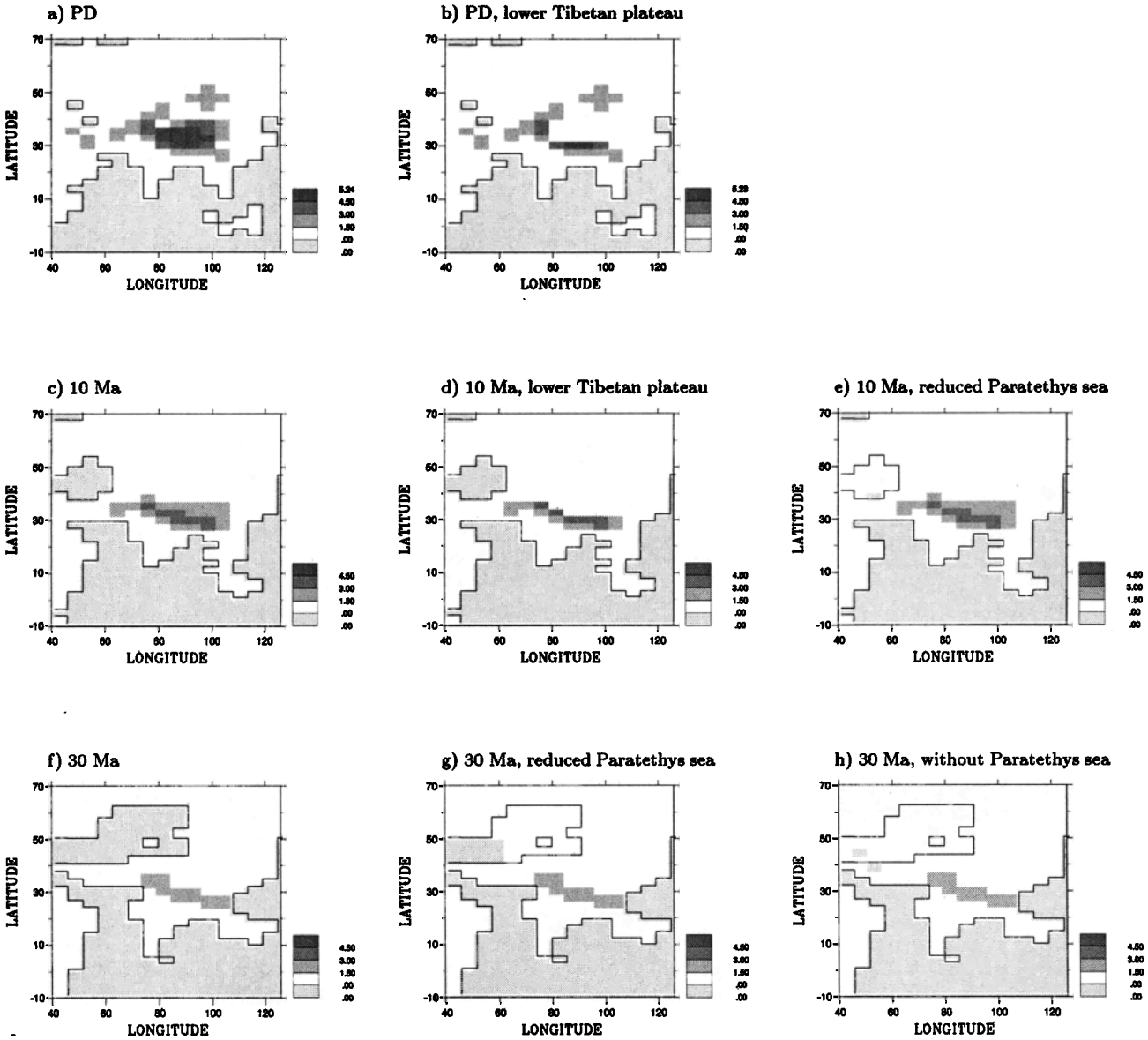

Figure 7. Paleogeography used for (a, c, f) "realistic" and (b, d, e, g, h) sensitivity experiments for (b) present day, for (d, e) middle-late Miocene, and for (g, h) Oligocene. Light grey represents oceanic areas, white represents the plain and relief lower than 1000 m. Grey scale shows the relief. (a) PD - Exp0, (b) PD - Exp3 - reduced Tibetan plateau, (c) 10 Ma - Exp1, (d) 10 Ma - Exp4- reduced Tibetan plateau, (e) 10 Ma - Exp5 - partial Paratethys retreat, uplifted Himalayas, (f) 30 Ma - Exp2, (g) 30 Ma - Exp6 - partial Paratethys retreat, and (h) 30 Ma - Exp7 - no Paratethys Sea.

al., 1986; *Harrison et al.*, 1992; *France-Lanord et al.*, 1993]. Exp3 (Figure 7b) tests the PD impact of the Tibetan plateau. The mean elevation of the Tibetan plateau of some 5000 m in the PD run (Exp0) is reduced to 1000 m in Exp3. In Exp4 (Figure 7d), we have also reduced the elevation of the Tibetan plateau at about 1000 m but on the 10 Ma paleogeographic map.

The shrinkage of the Paratethys epicontinental sea leads to the strengthening of a continental climate regime over much of Eurasia [*Ramstein et al.*, 1997a]. To quantify its impact on the monsoon, we have performed three sensitivity experiments (Table 1b). In Exp5 (Figure 7e), we have performed a simulation using the 10 Ma paleogeographic map (Exp1), in which we nearly suppress the Paratethys Sea. In Exp6 (Figure 7g), we have removed from the 30 Ma map (Exp2) the eastern part of the Paratethys Sea until its dimension at 10 Ma and replaced it by a low plain. Finally, the Paratethys Sea in Exp7 (Figure 7h) is completely removed from the 30 Ma map with the exception of oceanic basins corresponding to the PD Caspian and Black Seas.

The goals of these sensitivity experiments are (1) to investigate the impact of the Tibetan uplift (Exp3 and Exp4), (2) to see whether the amplitude of the shrinkage induces a linear response of the monsoon (Exp6 and Exp7), and (3) to show if local feedback over the Himalayas is a function of the elevation of this chain and is able to amplify climatic changes (Exp5 and Exp7).

We have used the "monsoon index" defined by *Prell and Kutzbach* [1987] to quantify the intensity of the monsoon, which can be approximated by the pressure gradient between the

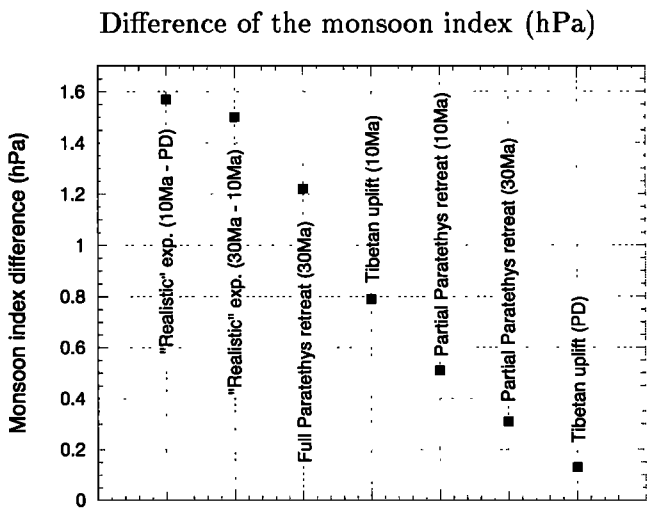

Figure 8. Differences of monsoon index in response to paleogeographic impact. Vertical scale is in hPa.

continent (Asia) and the adjacent ocean (Indian Ocean). This index equals the difference of mean sea level pressure between the Asian continent and the Indian Ocean, averaged in an area stretching between 45°E-120°E and 15°S-45°N. This zone includes both the Indian monsoon low-pressure cell, advecting wet air masses, and the Indian Ocean high-pressure cell.

We show in Figure 8, the computed monsoon index differences for the different simulations: the "realistic" paleogeographic changes between Oligocene, Miocene, and PD induce a nearly similar (strong) increase of the monsoon index (1.57 hPa and 1.5 hPa for Exp0-Exp1 and Exp1-Exp2, respectively). The sensitivity experiments show that the strongest increase of monsoon index (1.22 hPa) results from a full retreat of the Paratethys Sea in the Oligocene environment (Exp7-Exp2). In comparison, a partial Oligocene Paratethys retreat (Exp6-Exp2) strengthens this index by only 0.31 hPa. The retreat of this sea in the Miocene (Exp5-Exp1) increases this index by a higher 0.51 hPa value. The uplift of the Tibetan plateau at 10 Ma (Exp1-Exp4) enhances the monsoon index by 0.79 hPa. Finally, the effect of the altitude of the Tibetan plateau appears negligible in the PD experiment (Exp0-Exp3), with an increase of only 0.13 hPa.

A full shrinkage of the epicontinental sea (Exp7-Exp2) induces stronger heating of Eurasia and the extent of the thermal low pressure toward central Asia, and western Siberia (and also Arabia). The full retreat of the Paratethys Sea induces a stronger climatic change than a partial retreat (Exp6-Exp2) due to a more efficient summer heating.

The uplift of the Tibetan plateau mainly modifies the amplitude and location of the minimum of the low-pressure cell without modifying entirely its spatial development (Exp1-Exp4). We notice that the uplift of the Tibetan plateau in a PD experiment (about 4000 m) increases the monsoon index by only 0.13 hPa, 6 times less than in the 10 Ma run (Exp1-Exp4, 0.79 hPa), despite a weaker uplift (about 1500 m on average). To attempt to solve this contradiction, we have examined the development of the monsoon low-pressure cell, with and without the Tibetan plateau in the PD (Exp0 and Exp3) and 10 Ma (Exp1 and Exp4) simulations. The PD run (Exp0) presents two sea level pressure minimums, one over northwestern India, resulting from sensible heating, and the other over the eastern flank of the Tibetan plateau, resulting from latent heat release. With a reduced Tibetan plateau in a PD land-sea distribution (Exp3), the low-pressure minimum located over its eastern flank weakens (because of less precipitation), whereas the Indian trough remains unchanged. Precipitation increases over India because advection toward the eastern Tibetan flank is reduced. The high-pressure cell located over the Tibetan plateau also weakens. In a 10 Ma experiment (Exp1), the elevation of the Tibetan plateau and the presence of a smoothed slope inhibit the emergence of a low-pressure minimum over its eastern flank. There is only a minimum located over northwestern India. With a reduced Tibetan plateau (Exp4), the whole low-pressure cell increases. The impact of the uplift is widely linked to the development of the monsoon low-pressure cell.

These results point out that two thirds of the monsoon index increase from the Oligocene to PD is due to the combination of the full retreat of the Paratethys Sea and of the Tibetan plateau uplift. Although this result suggests that both the shrinkage and the Tibetan uplift are the main causes of the monsoon changes, the retreat of the Paratethys Sea alone plays a major role in large-scale atmospheric changes.

We have shown previously in the "realistic" experiments that the precipitation shifts northwestward from Indochina toward the Himalayas. To quantify now the influences of the geologic events on the precipitation evolution, we have defined two areas of land points. The first stretches over southern India and Indochina (area A: 65°E-120°E; 0°-20N), regions in which precipitation mainly occurs during the Oligocene. The second covers northern India, the Himalayas, and the Tibetan plateau up to southern China (area B: 65°E-120°E; 20°N-40°N) in which heavy rainfall occurs for the PD run.

To show the impact of the different forcing factors, we have plotted the mean summer precipitation over areas A and B, as a function of the monsoon index (Figure 9a). We point out that the intensification of the monsoon index corresponds to a redistribution of the rainfall over both areas. An increase in the monsoon index strengthens the precipitation over the northern area (box B, the lower group of points) and depletes the southern part (box A, the upper group of points).

To further investigate the impact of these geologic events, Figure 9b shows the variation of precipitation as a function of the monsoon index changes for the different forcing factors. No forcing factor tested in our sensitivity experiments is able to account for the increase of precipitation over the northern part (box B) (Exp0 [PD]-Exp2 [30Ma], +1.65 mm/d) or the decrease of precipitation over the southern part (box A) (-2.25 mm/d). The impact of the Tibetan plateau uplift in the 10 Ma runs (Exp1-Exp4) is strong enough to produce about one half of the precipitation decrease from 30 Ma to PD (1.2 mm/d) in the southern area and one half of the precipitation increase from 30 Ma to 10 Ma over the northern area (0.5 mm/d). Moreover, this increase mainly affects the eastern flank of the Tibetan plateau and northern Indochina, and less the Himalayas.

The Tibetan plateau uplift in the PD run (Exp0-Exp3) induces weak precipitation decrease over the northern area (-0.2 mm/d) and relatively strong changes over the southern part (-1.7 mm/d). However, as in the 10 Ma run, precipitation increases over the eastern flank of Tibet, while a broad decrease occurs over India and Indochina. This change reflects the slowing down of the westerlies over India and the increase of moisture convergence along the eastern flank of the Tibetan plateau.

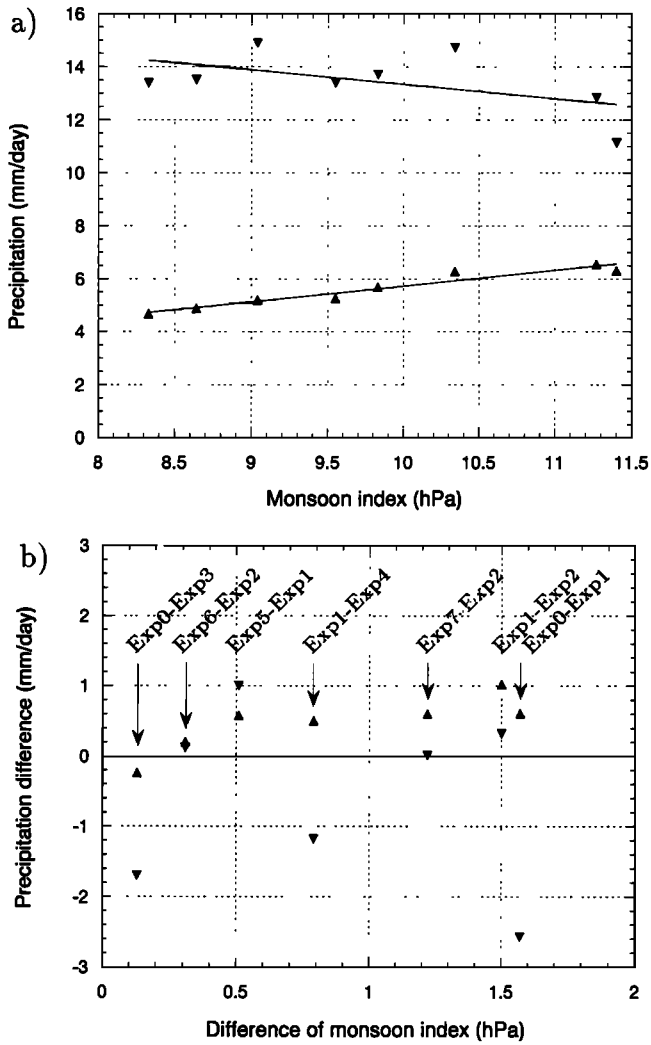

Figure 9. (a) Mean summer precipitation averaged over northern and southern Asian areas as a function of monsoon index. The horizontal scale is in hPa; the vertical scale is in mm/d. The upper (lower) group of points represents the mean precipitation averaged in box A (box B). (b) Mean precipitation variation as a function of the mean variations of monsoon index. The horizontal scale is in hPa; the vertical scale is in mm/d. For each experiment, the upper (lower) point represents precipitation change in box B (box A). Same notation as Figure 8.

In comparison to the Tibetan plateau uplift, the full retreat of the Paratethys Sea (Exp7-Exp2) strengthens precipitation over the northern part (+0.6 mm/d) and especially over the Himalayas, whereas there is no apparent rainfall change over the southern part (0 mm/d). In fact, a difference may be observed between the center of India (intensification) and Indochina (weakening) within box A (Figure 9) as reported by *Ramstein et al.* [1997a] because of the westward shift of the monsoon low-pressure cell resulting mainly from the Paratethys retreat. Actually, the influence on precipitation of the Paratethys Sea is also closely connected to orographic elevation. The rainfall strengthening (+0.58 mm/d) over the northern area (mainly over the Himalayas) in response to a partial shrinkage of the Paratethys Sea in the 10 Ma experiment (Exp5-Exp1) is as strong as in response to a full retreat (+0.6 mm/d) in a 30 Ma configuration (Exp7-Exp2) or stronger than in response to the Tibetan uplift (Exp1-Exp4) (+0.5 mm/d). We suggest that the impact of the Paratethys Sea retreat (Exp5-Exp1) on precipitation in the northern box depends strongly on dynamic feedback over the Himalayas. The Paratethys partial shrinkage (Exp5-Exp1) strengthens the moisture transport over northern India and the Himalayas, while increasing precipitation over its southern flank. An elevated range compels air masses to rise and to produce heavy precipitation along the slope. The latent heat release implies important convective motions, which act as a positive feedback to increase moisture convergence. This feedback may explain the amplification in precipitation observed in both Figures 9a and 9b. Conversely, a low mountain range reduces this dynamic feedback.

Thus we are able to reproduce partially the precipitation changes occurring in the realistic experiments with the sensitivity runs (-2.25 mm/d in the southern area, +1.65 mm/d in the northern area). However, no obvious dominant forcing factor emerges as a sole explanation for the monsoon precipitation changes. Both the Tibetan uplift and Paratethys retreat should be taken into account to reproduce the precipitation changes over southern Asia. However, we suggest that the impact of the Paratethys Sea retreat constitutes the most efficient factor to enhance precipitation over the Himalayas, but it depends strongly on the elevation of this chain.

6. African Monsoon

At present, the northern part of the African continent is divided into two main climatic areas: desert northward of 20°N and savanna/tropical forest south of 20°N, where the summer monsoon occurs. The long-term evolution of north African climate is only based on rare and poorly dated paleoclimatic indicators [*Ruddiman et al.*, 1989a]. Nevertheless, the progressive aridification of this area during the Cenozoic period is usually accepted and leads to the emergence of desert in north Africa in the late Miocene [*Axelrod and Raven*, 1978; *Sarnthein et al.*, 1982; *Robert and Chamley*, 1987; *Maley*, 1996].

6.1. Simulations of African Monsoon Changes

We have first simulated climatic changes between the Oligocene and PD, over a band of longitude covering 0°-30°E. This band does not account for the northerlies blowing along the Atlantic Coast and the area of heavy precipitation on the Ethiopian highlands, which may hide the monsoon, changes over inner Africa. We use values averaged in June-July-August-September (JJAS) with the aim of covering more accurately the monsoon season. During JJAS over this area, precipitation decreases by 30% and evaporation by 17% between the Oligocene (Exp2) and PD (Exp0). Besides the weakening of the monsoon, a time redistribution of the monsoon rainfall occurs. In the Oligocene experiment (Exp2), we observe two distinct phases, interrupted by a slight break in June. Only one phase exists at PD (Exp0). This break is amplified if we observe the precipitation minus evaporation (Figure 10) because of the high evaporation rate and the weaker precipitation decrease. To compensate this effect, the local recycling of moisture strengthens by 10% during this break at the expense of advection.

The zonal mean average JJAS precipitation shows that the monsoon is centered at 11.2°N for the PD simulation and at 14°N for the Oligocene experiment (Figure 11). This northward drift of

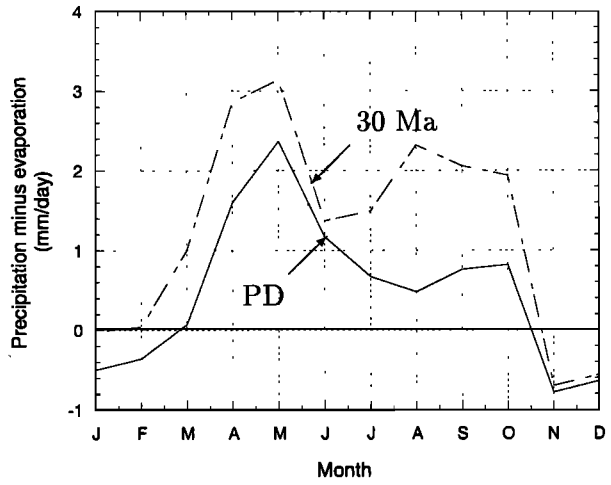

Figure 10. Monthly mean differences between precipitation and evaporation (mm/d). The solid (dashed) line represents the PD (30 Ma) experiment. Negative values indicate periods with evaporation exceeding precipitation.

2.8° reaches more than 3° during August, which defines the precipitation maximum simulated during the Oligocene monsoon. The northern limit of the precipitation belt, defined by the 2.5 mm/d threshold averaged on JJAS, is located at 15.3°N for PD and 22.1°N for the Oligocene (Figure 11). The JJAS northern limit shifts northward by 6.8°, and >8° in September. These results show that the Oligocene monsoon stretches northward without significantly shifting the position of the strongest precipitation.

Using the evaporation over precipitation ratio, we may show that the Asian monsoon precipitation is mainly driven by advection of moisture, whereas local recycling plays only a minor role. For the African monsoon, we observe a strong local recycling for PD and 30 Ma. Between the Oligocene and PD, precipitation weakening (-30%) is almost equally shared between advection (-17%) and local recycling (-13%) decreases.

6.2. Link Between Atmospheric Circulation and Paleogeographic Evolutions

At large spatial scales, the sea level pressure evolution (Figure 12) explains monsoon precipitation and advection changes. In the Oligocene experiment, because the continent is in a more southern position, the low-pressure cell, located over southern equatorial Africa, moves over western Africa as early as March (Figure 12a), whereas this position is reached a month later in the PD experiment (Figure 12b). As soon as the trough reaches western Africa, the winds reverse and advect moisture from the Gulf of Guinea and the Atlantic Ocean, which induce the first period of precipitation. At the end of the spring season in the Oligocene simulation, the monsoon low-pressure cell shifts northward, following the location of the strongest insolation. The insolation maximum migrates above northern Africa close to 20°N, inducing a strong heating of this area as well as the northward drift of the monsoon low-pressure cell (Figure 12c). However, because of the more southerly position of Africa, the low-pressure cell is blocked by the high-pressure belt of the Tethys seaway, which in turn, leads to a weakening of the monsoon trough (Figure 12c). Thus the moisture advection weakens, and the month of June experiences a decrease in monsoon intensity (Figure 10) (this does not occur in the PD simulation (Figure 12d)). The following months undergo a southern position of the insolation maximum: thus the thermal low-pressure cell drifts southward and deepens. We observe a new phase of heavy precipitation lasting from the months of July to October, with an intensification of advection. However, the low-pressure cell in the Oligocene experiment (Figure 12e) is weaker than the one developed for the PD (Figure 12f), although it advects more moisture. We attribute this apparent paradox to the characteristics of the low-pressure cell and to its link with the Asian low-pressure cell. In the Oligocene experiment (Figure 4a), the Tethys seaway generates a large ridge, separating the Asian thermal low-pressure cell from the African one, whereas in the PD experiment, the Asian-African monsoon system is strongly connected (see section 7).

These paleogeographic changes also modify the midtroposphere circulation and may induce feedback on the evolution of precipitation patterns. According to *Flohn and Nicholson* [1980] and *Ruddiman et al.* [1989], a stronger tropical easterly jet over Africa should enhance both rising motion and the precipitation over tropical Africa, and subsidence and drying over northern Africa. We do not observe all these features simultaneously. In our case, we observe an increase of the tropical easterly jet over Africa at 700 hPa between the Oligocene (4m/s) (Figure 13a) and the PD (8 m/s) (Figure 13b). However, this jet is associated with a spatial shrinkage of the ascending motions over tropical Africa covering 7.5° in latitude in the PD experiment and 17° for Oligocene, whereas we do not observe any changes in the jet intensity. For the Oligocene, a dry and smaller in size subsidence is located above the northern African Coast and the Tethys seaway (Figure 14a), whereas in the PD run, this subsidence covers a large part of the northern Africa and the Mediterranean Sea with a maximum over western Egypt (Figure 14b). The paleogeographic changes also disturb the westerlies in the upper troposphere at 300 hPa. This jet is located at 50°N for the PD and at 30°N in the Oligocene. The southward position of the westerlies near the tropical easterlies increases both the wind gradient in the upper troposphere and the shear stress. Although these features may play a role in African

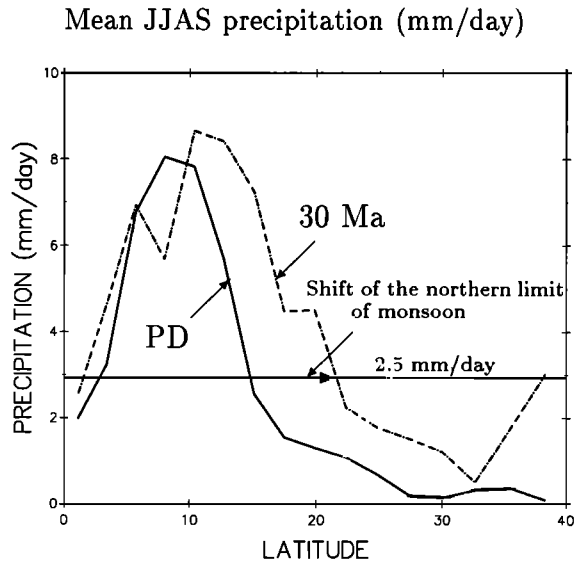

Figure 11. Mean JJAS zonal precipitation (mm/d) averaged between 0° and 30°E at PD (solid line) and 30 Ma (dotted line).

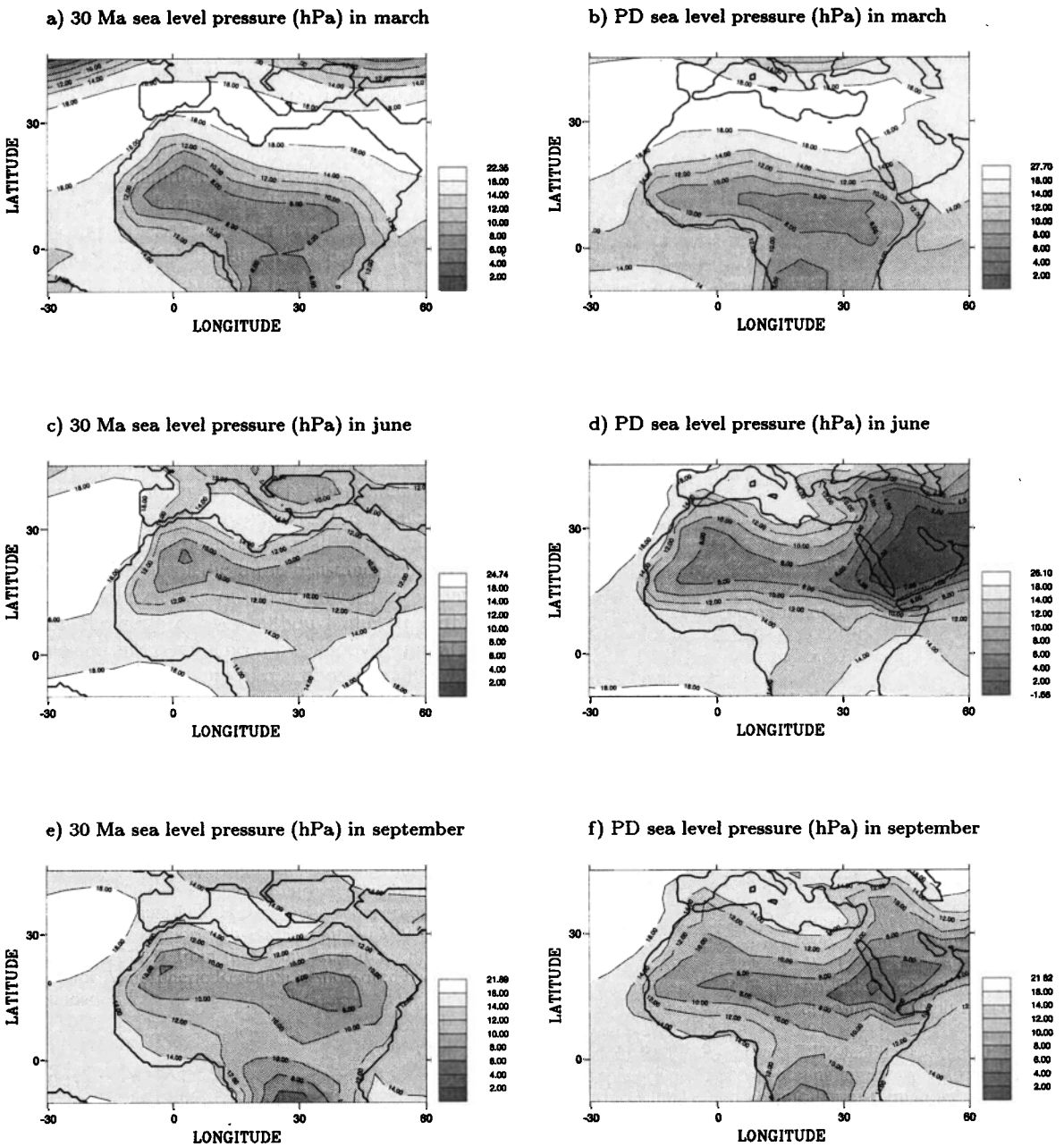

Figure 12. Sea level pressure (minus 1000 hPa) over Africa for the Oligocene (left) and PD (right). The gray areas represent the low-pressure cell, and white indicates pressure greater than 18 hPa (1018 hPa): (a) 30 Ma- Exp2 in March, (b) PD - Exp0 in March, (c) 30 Ma- Exp2 in June, (d) PD - Exp0 in June, (e) 30 Ma - Exp2 in September, and (f) PD - Exp0 in September.

monsoon evolution, further analysis would be beyond the scope of this paper.

6.3. Model Results and Proxy Data

Rain forests and savanna may have existed over a large part of northern Africa during the Oligocene and early Miocene periods [*Axelrod and Raven*, 1978; *Maley*, 1996], although evidence is limited [*Ruddiman et al.*, 1989]. During the Oligocene, because Africa was more to the south than today, these forests have been associated with a stronger monsoon invading this continent far inland [*Axelrod and Raven*, 1978]. The presence of an important draining system during the Cenozoic has been observed through remote sensing images [*Burke and Wells*, 1989]. The stretching of the monsoon over north Africa is driven by the continental drift of western Africa. According to *Axelrod and Raven* [1978], tropical forests extend both northward and southward, whereas *Pickford* [1992] proposes that the southern continental drift is the cause of a northwards stretching of the monsoon and of a drying of PD equatorial Africa (Congo, Zaire).

Using our numerical experiments, we investigated the impact of continental drift on climate using the following climatic parameters: precipitation, temperature, and Köppen's classification [*Köppen*, 1923]. This climatic classification is based on the comparison of the mean monthly precipitation and mean monthly temperature with empirical criteria [*Köppen*,

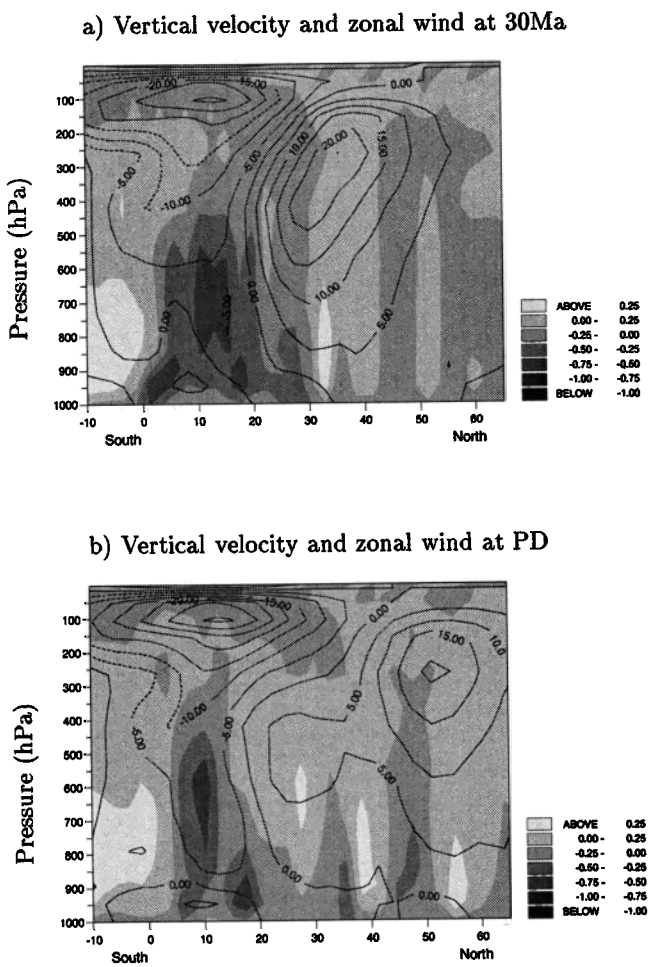

Figure 13. The mean vertical velocity (m/s) and the zonal wind field (m/s) in summer (JJAS) averaged over Africa between 0° and 30°E at (a) 30 Ma (Exp2) and (b) PD (Exp0). The vertical scale is pressure (hPa) and represents the atmosphere from sea level to 30 km height. Light gray is attributed to subsidence (positive values), and dark gray indicates ascending motion (negative values). The isolines represent the intensity of the zonal component wind. The interval between isocontours is 5 m/s.

1923; *Guetter and Kutzbach*, 1990]. We try to determine if a shift and shrinkage of the monsoon belt or an extension of tropical forest is confirmed by our results.

We thus compared the PD simulation with that of the Oligocene in order to optimize the climatic changes by defining three areas. The tropical area (A) (0°N-20°N, 15°W-45°E) is influenced by the African summer monsoon. The northern area (B) (20°N-33°N; 15°W-45°E) defines the PD dry area. Finally, to test the hypotheses, the shift [*Pickford*, 1992] versus the spreading of the monsoon belt hypothesis [*Axelrod and Raven*, 1978], we use a southern box (C) (-20°S-0°N, 15°E-45°E).

To present the climatic changes, we give the mean monthly precipitation averaged over each box, as well as the annual and summer temperature changes. The mean summer value is averaged over JJAS. To infer the climatic changes, we calculated the percentage of climatic types covering each area for both periods using Koppen's classification. We report these results in Table 2.

For tropical Africa (area A) (Figure 15a), the JJAS monsoon precipitation decreases by 1.5 mm/d (-24%) between the Oligocene (Exp2) and the PD (Exp0). Drastic reductions also occur during spring (-30%) and autumn (-36%), which are related to a shortening of the monsoon season by a month in spring and in autumn. In the Oligocene experiment, heavy rainfall is simulated until the month of October. Between the Oligocene and PD, temperature averages increase by +2.2°C for the annual mean and by +3.3°C during the monsoon. Less than +0.7°C of this change may be explained by the difference of mean elevation (using a mean lapse rate equal to 6°C/km). However, a large part of this warming is due to cloudiness reduction, especially in convective clouds, and reflects a decrease in monsoon precipitation. Using Köppen's classification, we do not see any clear transition. The extent of tropical forest along the Gulf of Guinea is reduced and replaced by savanna, which suggests a winter dry period. This result is confirmed by the increase of graminea during the Miocene [*Morley and Richards*, 1993]. The Sahelian region, between 15°N and 20°N, experiences the southward retreat of monsoon; savanna is mainly replaced by dryer biomes (steppe and desert). These results are in agreement with the evolution of vegetation suggested by Axelrod [*Axelrod and Raven*, 1978]. Savanna is largely reduced and replaced by desert and steppe, which confirms by the evolution of paleoenvironment in Sudan [*Awad and Breir*, 1993]. This drying is also reflected by the decrease of the kaolinite content in the sediment deposited in the Atlantic Ocean [*Robert and Chamley*, 1987].

For northern Africa (area B) (Figure 15b), changes are very different: summer precipitation decreases dramatically by 0.9 mm/d (-70%) due to a southward retreat of the monsoon. Annual warming of 1.6°C hides a significant summer warming of some 4.6°C. The difference in mean elevation between 30 Ma and PD decreases temperature by only 0.1°C. Two major events may lead to this warming: first, a southward retreat of monsoon which implies a decrease in cloudiness from 30 Ma to PD, leading to an important aridification, especially in the southern part of this area; second, a decrease of moisture advection due to changes in the low-pressure cell, which induces arification of the northwestern African Coast. This aridication, marked by a decrease in precipitation and a warming trend, leads to a clear reduction of steppe and savanna and to the emergence of desert. These results are confirmed by the southward retreat of the savanna [*Axelrod and Raven*, 1978] during the late Cenozoic and the presence of desert along the western Atlantic Coast [*Sarnthein et al.*, 1982]. Nevertheless, local discrepancies occur over northern Africa. For instance, in the Oligocene run, we simulate steppe instead of monsoon forest in northeastern Africa [*Bown*, 1982] and savanna instead of tropical forest in southwestern Libya [*Maley*, 1996], suggesting too weak precipitation.

For the last area (box C) (Figure 15c), the climatic changes are rather weak except in autumn. This is in agreement with an insignificant drift of eastern Africa. The summer warming (+0.55°C) may be explained by the mean elevation difference, which increases temperature (by 0.6°C). No drastic vegetation transition occurs. For the Oligocene run, savanna increases slightly and the desert along the southwestern African Coast remains nearly unchanged, in good agreement with the eolian record in deep-sea sediment cores in the Indian ocean [*Hovan and Rea*, 1992].

The geographic patterns of these changes suggest that the northward drift of Africa since 30 Ma drives the retreat of the monsoon in a thin belt inside areas A and B. Climatic changes (warming and drying) in these areas consist mainly in the drying

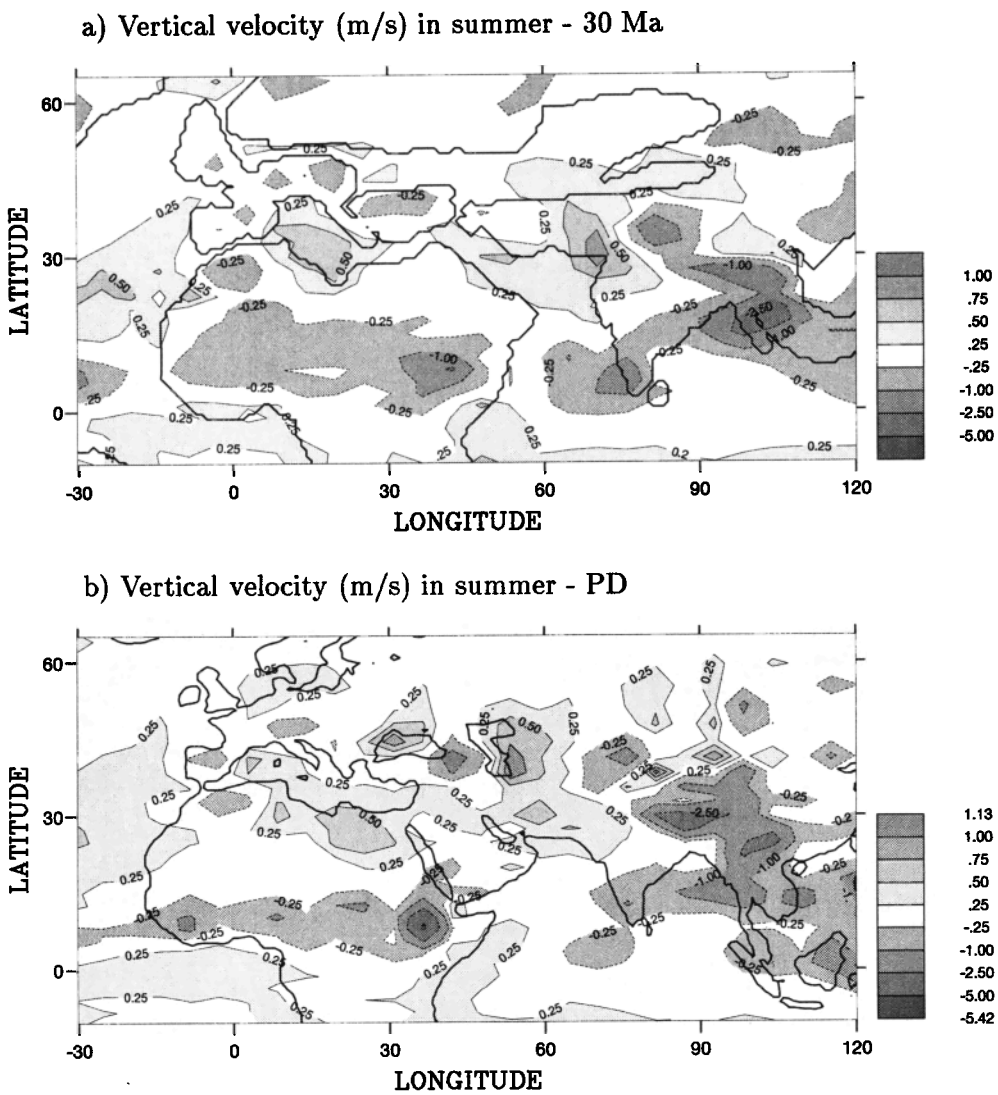

Figure 14. Mean vertical velocity (m/s) in summer at 500 hPa (≈4500 m) at (a) 30 Ma (Exp2) and (b) PD (Exp0). Isolines are plotted for -5, -2.5, -1, -0.25, +0.25, +0.5, +0.75, and +1 m/s. Gray color represents vertical motion greater than ±0.25 m/s. Dotted line indicates ascending flow, and solid line shows subsidence.

of the subtropical area between 15°N and 20°N. Climatic variations in these areas confirm the shrinkage of the monsoon. These results are in favor of Axelrod's assumption which suggested a stretching [*Axelrod and Raven*, 1978] of the African monsoon. In response to the northward motion of Africa, precipitation changes mainly affect subtropical Africa (20°N), whereas rainfall in equatorial Africa (area C) is not greatly reduced. However, because of the presence of a dry season (when evaporation exceeds precipitation), the formation of evaporites is possible, as shown by *Pickford* [1992] in Uganda for the Miocene. Although paleogeographic changes are able to reduce strongly the monsoon area and replace it by an arid climate, other mechanisms such as albedo evolution and CO_2 decrease also play an important part.

7. Links Between the African and Asian Monsoon Systems

In section 6.2, we compare the seasonal evolution of the African low-pressure cell between the Oligocene and PD, and point out the role of the Tethys seaway to separate the Asian and African thermal low-pressure cells. For the Oligocene, the African low-pressure cell develops two pressure minima associated with two heating areas, one located over northwestern Africa and the other over northeastern Africa (Figure 4a). These two maxima of heating advect moisture from the Atlantic Ocean and western Eurasia, whereas in the PD experiment, moisture is only advected from the Atlantic Ocean via the African trough and by the minimum of pressure, also associated with a maximum of heating over Arabia (Figure 4c). This low-pressure cell configuration explains the weak convergence toward the inner continent. This split of the monsoon system from the PD to the Oligocene is also found using another LMD version (LMD4ter) at lower resolution 48x36 coupled or not with a slab ocean [*Ramstein et al.*, 1997a].

Flohn and Nicholson [1980] and *Ruddiman et al.* [1989] suggested that the strengthening of the African tropical easterly jet is linked to the Tibetan plateau uplift because it strongly diverts the midlatitude westerlies southward, which then merge with the tropical easterly jet over Arabia. This mechanism is also

Table 2a. The Climatic Evolution Over Tropical Africa

Climate in Area A	PD (Exp0), %	30 Ma (Exp2), %
Warm and everwet	0.9	2.7
Warm and summerwet	31.6	53.1
Warm temperate and winterwet	0	0.9
Warm temperate	2.6	8.8
Semiarid	14.9	26.6
Arid	50	7.9

Table 2c. The Climatic Evolution Over South Tropical Africa

Climate in Area C	PD (Exp0), %	30 Ma (Exp2), %
Warm and everwet	4	0
Warm and summerwet	92	76.7
Warm temperate and summerwet	0	10
Semiarid	0	3.3
Arid	4	10

found in our PD simulation (not shown). The easterly jet located above the Indian subcontinent and the Arabian Sea merges with the midlatitude westerly jet diverted by the Tibetan plateau toward Arabia, feeding the tropical easterly jet at 500 hPa over Africa (Figure 13b). In the Oligocene experiment, the midlatitude westerly jet is poorly diverted for two reasons, namely, the absence of Tibetan plateau and the presence of inland seas (the Paratethys Sea and the Tethys seaway) which drives atmospheric flow located at 20°N zonally (Figure 13a). The weak release of latent heat over the Himalayas reduces the rising air masses (Figure 5a). For these reasons and also in response to a strong westerly jet driven by the Tethys seaway, the India/Himalayan easterly jet is not generated (Figure 13a).

8. Conclusions

In this paper, we have shown that paleogeographic changes, orogenic episodes, plate motion, and sea level changes are able to reproduce the major trends of the monsoon evolution in Africa and in Asia during the past 30 Myr. Until now, the Tibetan plateau uplift was considered to be the major cause of the summer Asian monsoon [*Kutzbach et al.*, 1989; *Prell and Kutzbach*, 1992]. In this paper, we highlight the role of the progressive shrinkage of the Paratethys Sea on the Eurasian climate and the Asian monsoon. The Paratethys retreat stretches, deepens, and shifts northwestward the monsoon low-pressure cell, modifying the large-scale circulation and thus the monsoon precipitation pattern. Precipitation decreases over Indochina and increases over the southern flank of the Himalayas and central India. These changes are in agreement with proxy data [*Ducrocq et al.*, 1994] and imply that Indochina has experienced no significant climatic changes since the early Miocene, while the Himalayas have experienced an increase in precipitation during the late Miocene. In addition to changes in precipitation, the 850 hPa wind field reveals a strengthening over the Arabian Sea and a weakening of winds over Bengal Bay from 30 Ma to PD. The location of the strong westerly jet over the Arabian Sea may be compared with the upwelling intensity deduced from foraminifera development recorded in sediment cores [*Kroon et al.*, 1991; *Nigrini and Caulet*, 1992; *Prell et al.*, 1992]. An abrupt increase in the foraminifera population during the late Miocene has been attributed to the "onset" of the modern monsoon [*Kroon et al.*, 1991]. However, the foraminifera in the sediment core is an indicator of the evolution of winds, only above the drilling site, whereas our simulations are able to point out the global spatial pattern of the wind field evolution. Our experiments reveal a northward shift of the monsoon winds over the Arabian Sea. Therefore we suggest that this apparent onset of the monsoon observed in the upwelling record reflects the northward shift of the monsoon winds over the Arabian Sea.

Table 2b. The Climatic Evolution Over Northern Africa

Climate in Area B	PD (Exp0), %	30 Ma (Exp2), %
Warm and summerwet	0	15.9
Warm temperate and winterwet	0	3.2
Warm temperate and summerwet	0	15.8
Warm temperate	1.2	1.6
Semiarid	13.6	44.4
Arid	85.2	19.1

Besides the evolution in the spatial pattern of rainfall, our simulations reveal changes in the seasonal distribution of precipitation and in the monthly heavy-rain frequency during summer over the Himalayas. We have also introduced the runoff, the seasonal distribution of precipitation, and the monthly heavy-rain frequency because they play important roles and they help to better explain the sedimentary process. The role of heavy rainy events appears to be predominant in physical erosion.

We quantify the respective impact of the Paratethys shrinkage and of the Tibetan uplift on the Asian summer monsoon by performing sensitivity experiments. These experiments reveal that both the Paratethys shrinkage and the Tibetan uplift increase precipitation over the Himalayas, northern India, and northern Indochina, whereas the southern part of Asia becomes drier. These experiments also reveal that a complete retreat of the Paratethys Sea induces a precipitation increase over the Himalayas stronger than the precipitation increase induced by the sole Tibetan plateau uplift. The precipitation increase over the Himalayas is weakly linked to the elevation of the Tibetan plateau as long as the Himalayas are already uplifted. We also show that the impact of the Paratethys shrinkage on the precipitation depends on the elevation of the Himalayas because of feedback mechanisms such as the latent heat release, which strengthens the moisture advection.

For the African monsoon we show that the northward drift of the continent and the closure of the Tethys seaway explain a large part of the summer monsoon evolution during the late Cenozoic. The southern location of Africa and the Tethys seaway splits the African and Asian monsoons into two separate systems, which explains the moisture advection far inland in Africa during the Oligocene. Moreover, comparing our simulations to different scenarios of monsoon evolutions [*Axelrod and Raven*, 1978; *Pickford*, 1992], we conclude that the northward drift of this continent leads to a shrinkage of the monsoon belt as suggested by *Axelrod and Raven* [1978]. At last, we show that during the Oligocene, due to the Tethys seaway, the Asian and African monsoon systems were clearly separated, whereas for the present day, our simulations point out a link between these monsoons at low and middle tropospheric levels.

The results presented here have been produced within a multidisciplinary approach between different fields of Earth

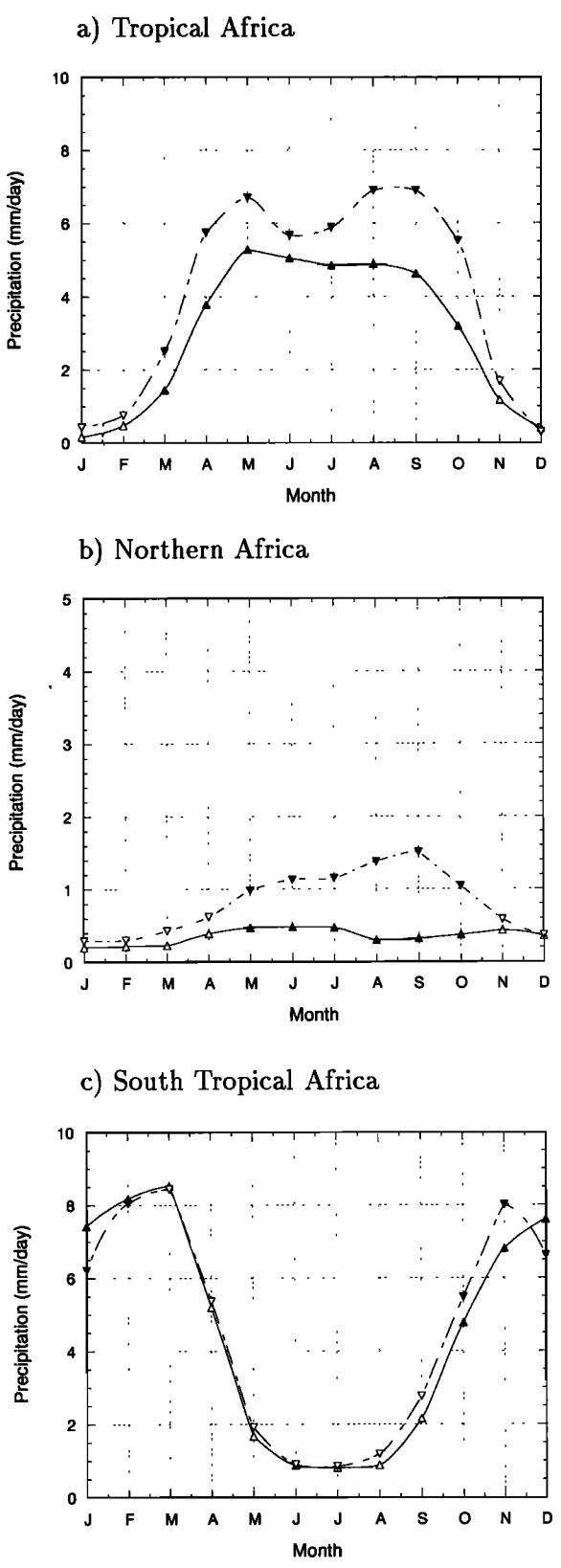

Figure 15. Monthly mean precipitation (mm/d) averaged over (a) tropical Africa, (b) northern Africa, and (c) south tropical Africa. The solid line with right-side-up triangle represents PD precipitation (Exp0); the dashed line with inverted triangle shows precipitation at 30 Ma (Exp2). Solid triangle indicates statistically significant changes; open triangles are for insignificant changes. The same vertical scale is used for Figures 15a and 15c; a different scale is used for Figure 15b.

science. This approach was necessary to allow the inclusion of other pieces of the puzzle in future simulations. Therefore these results are only expected to reproduce major climatic evolutions induced by paleogeographic changes. Accounting for realistic changes in carbon dioxide, oceanic circulation, and vegetation should obviously help to improve the model/data comparison. However at this stage, we consider that most of the main features of the monsoon evolution may be understood using realistic changes in paleogeography.

Acknowledgments. The authors wish to thank P. Bracconot, Y. Gaudemer, F. Métivier, N. de Noblet, and L.E. Ricou for helpful discussions. We also thank S. Gilder and M. Kageyama, who helped us to improve the English. This work was carried out using the IDRIS and CEA computing facilities. We thank J.Y. Peterschmitt for providing the postprocessing package. This work is supported by the French scientific program Dynamique et Transfert Terrestre, INSU. IPGP contribution 1581, LSCE contribution 175, and DTT-INSU contribution 157.

References

Achache, J., V. Courtillot, and Y. Zhou, Paleogeographic and tectonic evolution of southern Tibet since middle Cretaceous time: New paleomagnetic data and synthesis, *J.. Geophys. Res., 89*, 10311-10339, 1984.

Amano, K., and A. Taira, Two-phase uplift of higher Himalayas since 17 Ma, *Geology, 20*, 391-394, 1992.

Awad, M.Z., and F.A. Breir, Oligo-Miocene to Quaternary palaeoenvironment in Gezira area, central Sudan, in *Geoscientific Research in Northeast Africa: Proceedings of the International Conference (Berlin, 17-19 June 93)*, edited by U. Thorweile and H. Schandelmeier, pp.465-470, A.A. Balkema, Brookfield, Vt., 1993.

Axelrod, D.I., and P.H. Raven, Late Cretaceous and Tertiary vegetation history, in *Biogeography and Ecology of South Africa*, edited by M. Werger, Junk, The Hague, 1978.

Baker, B.H., Structure and evolution of Kenya Rift Valley, *Nature, 229*, 538-542, 1971.

Barazangi, M., and J. Ni, Velocities and propagation characteristics of Pn and Sn beneath the Himalayas and Tibetan plateau: Possible evidence for underthrusting of Indian continental lithosphere beneath Tibet, *Geology, 10*, 179-185, 1982.

Barron, E.J., and W.M. Washington, The role of geographic variables in explaining paleoclimates: Results from Cretaceous climate model sensitivity studies, *J. Geophys. Res., 89*, 1267-1279, 1984.

Berner, R.A., Palaeo-CO_2 and climate, *Nature, 358*, 114, 1992.

Besse, J., and V. Courtillot, Paleogeographic maps of the continents bordering in the Indian Ocean since the early Jurassic, *J. Geophys. Res., 93*, 11791-11808, 1988.

Besse, J., and V. Courtillot, Revised and synthetic apparent polar wander paths of the African, Eurasian, North-American and Indian plates, and true polar wander since 200 Ma, *J. Geophys. Res., 96*, 4029-4050, 1991.

Besse, J., V. Courtillot, J.P. Pozzi, M. Westphal, and Y.X. Zhou, Paleomagnetic estimates of Cenozoic convergence in the Himalayan thrusts and Zangbo suture, *Nature, 311*, 621-626, 1984.

Bird, P., Formation of the Rocky Mountains, western United States: A continuum computer model, *Science, 239*, 1501-1507, 1988.

Bown, T.M., Ichnofossils and rhizoliths of the nearshore fluvial Jebel Qatrani formation (Oligocene), Fayum Province, Egypt, *Palaeogeogr. Palaeoclim. Palaeoecol., 40*, 255-309, 1982.

Briais, A., P. Patriat, and P. Tapponnier, Updated interpretation of the magnetic anomalies and seafloor spreading stages in the South China Sea, *J. Geophys. Res., 98*, 6299-6328, 1993.

Burke, K., and G.L. Wells, Trans-African drainage system of the Sahara: Was it the Nile?, *Geology, 17*, 743-747, 1989.

Cerling, T.E., Late Cenozoic vegetation change, atmospheric CO_2, and tectonics, in *Tectonic Uplift and Climate Change*, edited by W.F. Ruddiman, pp. 313-325, Plenum, New York, 1997.

Cerling, T.E., J.M. Harris, B.J. MacFadden, M.G. Leakey, J. Quade, V. Eisenmann, and J.R. Ehleringer, Global vegetation change through the Miocene/Pliocene boundary, *Nature, 389*, 153-158, 1997.

Chase, S., The modern geoid and ancient plate boundaries, *Earth Planet. Sci. Lett., 62*, 314-320, 1983.

Chen, Y., V. Courtillot, J.P. Cogné, J. Besse, Z. Yang, and R. Enkin, The configuration of Asia prior to the collision of India: Cretaceous paleomagnetic constrains, *J. Geophys. Res.*, *98*, 21927-21941, 1993.

Chenggao, G., and R.W. Renaut, The effect of Tibetan uplift on the formation and preservation of Tertiary lacustrine source-rocks in eastern China, *J. Paleolimnol.*, *11*, 31-40, 1994.

Coleman, M., and K. Hodges, Evidence for Tibetan plateau uplift before 14 Ma from a new minimum age for east-west extension, *Nature*, *374*, 49-52, 1995.

Copeland, P., T.M. Harrison, W.S.F. Kidd, X. Ronghua, and Z. Yuquan, Rapid early Miocene acceleration of uplift in the Gangdese belt, Xizang (southern Tibet), and its bearing on accommodation mechanisms of the Indian-Asia collision, *Earth Planet. Sci. Lett.*, *86*, 240-252, 1987.

Curry, W.B., D.R. Ostermann, M.V.S. Guptha, and V. Ittekkot, Foraminiferal production and monsoonal upwelling in the Arabian Sea: Evidence from sediments traps, in *Evolution of the Upwelling Systems Since the Early Miocene*, edited by W.L. Prell and K.C. Emeis,. *Geol. Soc. Spec. Publ.*, *62.*, 1992.

De Noblet, N., P. Braconnot, S. Joussaume, and V. Masson, Sensitivity of simulated Asian and African summer monsoons to orbitally induced variations in insolation 126, 115 and 6 kBP, *Clim. Dyn.*, *12*, 589-603, 1996.

Dercourt, J., L.E. Ricou, and B. Vrielinck (Eds), *Atlas Tethys Palaeoenvironmental Maps*, 307 pp., Gauthier-Villars, Paris, 1993.

Derry, L.A., and C. France-Lanord, Himalayan weathering and erosion fluxes: Climate and tectonics controls, in *Tectonic Uplift and Climate Change*, edited by W.F. Ruddiman, pp. 289-312, Plenum, New York, 1997.

Diester-Haass, L., and R. Zahn, Eocene-Oligocene transition in the Southern Ocean: History of water mass circulation and biological productivity, *Geology*, *24*, 163-166, 1996.

Dong, B., P. Valdes, and N.M. Hall, The changes of monsoonal climates due to earth's orbital perturbations and ice age boundary conditions, *Paleoclim. Data Model*, *1*, 203-240, 1996.

Ducoudré, N., K. Laval, and A. Perrier, SECHIBA, a new set of parametrizations of the hydrologic exchanges at the land/atmosphere interface within the LMD atmospheric general circulation model, *J. Clim.*, *6*, 248-273, 1994.

Ducrocq, S., Y. Chaimanee, V. Suteethorn, and J.J. Jaeger, Ages and paleoenvironment of Miocene mammalian faunas from Thailand, *Palaeogeogr. Palaoeclim. Palaeoecol.*, *108*, 149-163, 1994.

Ehrmann, W.U., and A. Mackensen, Sedimentological evidence for the formation of an east Antarctic ice sheet in Eocene/Oligocene time, *Palaeogeogr. Palaeoclim. Palaeoecol.*, *93*, 85-112, 1992.

Emeis, K.C., D.M. Anderson, H. Doose, D. Kroon, and D. Schulz-Bull, Sea-surface temperatures and the history of monsoon upwelling in the northwest Arabian Sea during the last 500,000 years, *Quat. Res.*, *43*, 355-361, 1995.

Flohn, H., and S.E. Nicholson, Climatic fluctuations in the arid belt of the "Old World" since the last glacial maximum: Possible causes and future implications, *Palaeoecol. Africa*, *12*, 3-22, 1980.

Fouquart, Y., and B. Bonnel, Computations of solar heating of the Earth's atmosphere, *Beitr. Phys. Atmos.*, *53*, 35-62, 1980.

Frakes, L.A., J.E. Francis, and J.I. Syktus, *Climate Modes of the Phanerozoic*, Cambridge Univ. Press, New York, 1992.

Frakes, L.A., J.L. Probst, and W. Ludwig, Latitudinal distribution of paleotemperature on land and sea from early Cretaceous to middle Miocene, *C.R. Acad. Sci. Paris*, *318*, 1209-1218, 1994.

France-Lanord, C., and L. Derry, $\delta^{13}C$ of organic carbon in the Bengal fan : Source evolution and transport of C3 and C4 plant carbon to marine sediments, *Geochim. Cosmochim. Acta*, *58*, 4809-4814, 1994.

France-Lanord, C., L. Derry, and A. Michard, Evolution of the Himalayas since Miocene time: Isotopic and sedimentological evidence from the Bengal fan, in *Himalayan Tectonics*, vol. *74*, edited by P.J. Treloar and M. Searle, pp. 603-621, Geol. Soc., London, , 1993.

Guetter, P.J., and J.E. Kutzbach, A modified Köppen classification applied to model simulations of glacial and interglacial climates, *Clim. Change*, *16*, 193-215, 1990.

Hahn, D.G., and S. Manabe, The role of mountains in the south Asian monsoon circulation, *J. Atmos. Sci.*, *32*, 1515-1541, 1975.

Hallam, A., *An Outline of Phanerozoic Biogeography*, 246 pp., Oxford Univ. Press, New York, 1994.

Haq, B.U., Paleoceanography: A synoptic overview of 200 Million years of ocean history, in *Marine Geology and Oceanography of Arabian Sea and Coastal Pakistan*, edited by J.D. Milliman, and B.U. Haq, pp. 201-231, Van Nostrand Reinhold, New York, 1984.

Harrison, T.M., P. Copeland, W.S.F. Kidd, and A. Yin, Raising Tibet, *Science*, *255*, 1663-1670, 1992.

Harzallah, A., and R. Sadourny, Internal versus SST forced atmospheric variability as simulated by an atmospheric general circulation model, *J. Clim.*, *8*, 474-498, 1995.

Hastenrath, S., *Climate and Circulation of the Tropics*, 455 pp., D. Reidel, Norwell, Mass., 1985.

Hodges, K.V., R.R. Parrish, T.B. Housh, D.R. Lux, B.C. Burchfield, L.H. Royden, and Z. Chen, Simultaneous Miocene extension and shortening in the Himalayan orogen, *Science*, *258*, 1466-1470, 1992.

Hofmann, C., V. Courtillot, G. Féraud, P. Rochette, G. Yirgu, E. Ketefo, and R. Pik, Timing of the Ethiopian flood basalt event and implications for plume birth and global change, *Nature*, *389*, 838-841, 1997.

Hoorn, C., J. Guerrero, G.A. Sarmiento, and M.A. Lorente, Andean tectonics as a cause for changing drainage patterns in Miocene northern South America, *Geology*, *23*, 237-240, 1995.

Houseman, G.A., and P. England, Finite strain calculations of continental deformation, 1, Methods and general results for convergent zones, *J. Geophys. Res.*, *91*, 3651-3663, 1986a.

Houseman, G.A., and P. England, Finite strain calculations of continental deformation, 2, Comparison with the India-Asia collision zone, *J. Geophys. Res.*, *91*, 3664-3676, 1986b.

Hovan, S.A., and D.K. Rea, The Cenozoic record of continental mineral deposition on Broken and Ninety East ridges, Indian Ocean: Southern African aridity and sediment delivery from the Himalayas, *Paleoceanography*, *7*, 833-860, 1992.

James, I.N., *Introduction to Circulating Atmospheres*, 422 pp., Cambridge Univ. Press, New York, 1994.

Kennett, J.P., and L.D. Scott, Proteus and proto-oceanus: Ancestral paleogene oceans as revealed from Antarctic stable isotopic results; ODP leg 113, *Proc. Ocean Drill. Program Sci. Results*, *113*, 865-880, 1990.

Kennett, J.P., et al., Cenozoic paleoceanography in the southwest Pacific Ocean, Antarctic glaciation and the development of the circum-Antarctic current, *Initial Rep. Deep Sea Drill. Proj.*, *29*, 1155-1166, 1975.

Köppen, W., *Die Klimate der Erde*, Walter de Gruyter, Berlin, 1923.

Kroon, D., T. Steens, and S.R. Troelstra, Onset of monsoonal related upwelling in the western Arabian Sea as revealed by planktonic foraminifers, in *Proc. Ocean Drill. Program Sci. Results*, vol. 117, 257-263, 1991.

Kutzbach, J.E., P.J. Guetter, W.F. Ruddiman, and W.L. Prell, Sensitivity of climatic uplift in southern Asia and in the American West: Numerical experiments, *J. Geophys. Res.*, *94*, 18393-18407, 1989.

Kutzbach, J.E., W.L. Prell, and W.F. Ruddiman, Sensitivity of Eurasian climate to surface uplift of Tibetan plateau, *J. Geol.*, *101*, 177-190, 1993.

Kutzbach, J.E., W.F. Ruddiman, and W.L. Prell, Possible effects of Cenozoic uplift and CO_2 lowering on global and regional hydrology, in *Tectonic Uplift and Climate Change*, edited by W.F. Ruddiman, pp. 149-170, Plenum, New York, 1997.

Laskar, J., Secular evolution of the solar system over 10 millions years, *Astron. Astrophys.*, *98*, 341-362, 1988.

Leopold, E.B., G. Liu, and S. Clay-Poole, *Low-Biomass Vegetation in the Oligocene?*, Princeton Univ. Press, Princeton, N.J., 1992.

Li, Y., An apparent polar wander path from the Tarim block, China, *Tectonophysics*, *181*, 31-41, 1990.

Lorenz, C., et al., Late Rupelian (30 to 28 Ma), in *Atlas Tethys Palaeoenvironmental Maps*, edited by J. Dercourt, L.E. Ricou, and B. Vrielynck, pp. 211-233, Gauthier-Villars, Paris, 1993.

Maley, J., The African rain forest - Main characteristics of changes in vegetation and climate from the Upper Cretaceous to the Quaternary, *Proc. R. Soc. Edinburgh*, *104 B*, 31-73, 1996.

Métivier, F., Volumes sédimentaires et bilans de masses en Asie pendant le Cénozoïque, Ph.D. thesis, Univ. Paris 7, Paris, 1996.

Meyer, B., P. Tapponnier, L. Bourjot, F. Métivier, Y. Gaudemer, G. Peltzer, G. Shunmin, and C. Zhitai, Crustal thickening in Gansu Qinghai, lithospheric mantle subduction, and oblique, strike-slip controlled growth of the Tibet plateau, *Geophys. J. Int.*, *135*, 1-47, 1998.

Molnar, P., and P. England, Late Cenozoic uplift of mountain ranges and global climate change: chicken or egg?, *Nature*, *346*, 29-41, 1990.

Molnar, P., and J. Stock, Relative motions of hotspots in the Pacific,

Atlantic, and Indian oceans since late Cretaceous time, *Nature, 327*, 587-591, 1987.

Molnar, P., P. England, and J. Martinod, Mantle dynamics, uplift of the Tibetan plateau, and the Indian monsoon, *Rev. Geophys., 31*, 357-396, 1993.

Morcrette, J., Radiation and cloud radiative properties in the ECMWF forecasting system, *J. Geophys. Res., 96*, 9121-9132, 1991.

Morgan, W.J., Hotspot track and the rifting of the Atlantic, *Tectonophysics, 94*, 123-139, 1983.

Morley, R.J., and K. Richards, Graminae cuticle: A key indicator of the late Cenozoic climatic change in the Niger delta, *Palaeogeogr. Palaeoclim. Palaeoecol., 77*, 119-127, 1993.

Nagymarosy, A., From Tethys to Paratethys, a way of survival, *Acta Geod. Geophys. Mont. Hung., 25*, 373-385, 1990.

Nigrini, C., and J.P. Caulet, Late Neogene radiolarian assemblages characteristics of Indo-Pacific areas of upwelling, *Micropaleontology, 38*, 139-164, 1992.

Nürnberg, D., and R.D. Muller, The tectonic evolution of the South Atlantic from Late Jurassic to Present, *Tectonophysics, 181*, 27-33, 1991.

Oldow, J.S., A.W. Bally, H.G. Avé Lallemant, and W.P. Leeman, Phanerozoic evolution of the North American Cordillera; United States and Canada, in *The Geology of North America - An Overview*, edited by A.W. Bally and A.R. Palmer, pp. 139-232, Geol. Soc. of Am., Boulder, Colo., 1989.

Olivet, J.L., J. Bonnin, P. Beuzart, and J.M. Auzende, Cinénatique de l'Atlantique Nord et Central, *Rapp. Sci. Tech., 54*, Cent. Nat. Explor. Océans, Brest, 1984.

Orszag-Sperber, F., J. Butterlin, J. Clermonte, M. Colchen, R. Guiraud, R. Poisson, and L.E. Ricou, Tortonian (11 to 6.5 Ma), in *Atlas Tethys Palaeoenvironmental Maps*, edited by J. Dercourt, L.E. Ricou, and B. Vrielinck, pp. 243-258, Gauthier-Villars, Paris, 1993.

Otto-Bliesner, B.L., and G.R. Upchurch Jr., Vegetation-induced warming of high-latitudes regions during the Late Cretaceous period, *Nature, 385*, 804-807, 1997.

Partridge, T.C., Late Neogene uplift in eastern Africa and southern Africa and its paleoclimatic implications, in *Tectonic Uplift and Climate Change*, edited by W.F. Ruddiman, pp. 63-86, Plenum, New York, 1997.

Patriat, P., and J. Achache, India-Eurasia collision chronology has implication for crustal shortening and driving mechanism of plate, *Nature, 311*, 615-621, 1984.

Peltzer, G., and P. Tapponnier, Formation and evolution of strike-slip faults, rifts and basins during the India-Asia collision: An experimental approach, *J. Geophys. Res., 93*, 15095-15117, 1988.

Pickford, M., Evidence for an arid climate in western Uganda during middle Miocene, *C.R. Acad. Sci. Paris, 315*, 1419-1424, 1992.

Powell, C.M., and P.J. Conoghan, Tectonic models of Tibetan plateau, *Geology, 3*, 727-731, 1975.

Prell, W.L., and J.E. Kutzbach, Monsoon variability over the past 150,000 years, *J. Geophys. Res., 92* , 8411-8425, 1987.

Prell, W.L., and J.E. Kutzbach, Sensitivity of the Indian monsoon to forcing parameters and implications for its evolution, *Nature, 360*, 647-652, 1992.

Prell, W.L., R.E. Marvil, and M.E. Luther, Variability in upwelling fields in the northwestern Indian Ocean, 2; Data-model comparison at 9,000 years B.P., *Paleoceanography, 5*, 447-457, 1990.

Prell, W.L., D.W. Murray, S.C. Clemens, and D.M. Anderson, Evolution and variability of the Indian Ocean summer monsoon: Evidence from the Western Arabian Sea Drilling Program, in *Synthesis of Results From Scientific Drilling in the Indian Ocean, Geophys. Monogr. Ser.*, vol. 70, edited by R.A. Duncan et al., pp. 447-470, AGU, Washington, D.C., 1992.

Quade, J., T.E. Cerling, and J.R. Bowman, Development of Asian monsoon revealed by marked ecological shift during the latest Miocene in northern Pakistan, *Nature, 342*, 163-166, 1989.

Rack, F., A geologic perspective on the Miocene evolution fo the Antarctic Circumpolar Current system, *Tectonophysics, 22*, 397-415, 1993.

Ramstein, G., F. Fluteau, J. Besse, and S. Joussaume, Effect of orogeny, plate motion and land-Sea distribution on Eurasian climate over the past 30 million years, *Nature, 386*, 788-795, 1997a.

Ramstein, G., F. Fluteau, and V. Masson, Existence of an ice cap during the mid-Cretaceous period (120-90 Ma): An AGCM investigation, *Ann. Glaciol., 25*, 198-202, 1997b.

Rea, D.K., Delivery of Himalayan sediment to the northern Indian Ocean and its relation to global climate, sea level, uplift, and seawater strontium, in *Synthesis of Results From Scientific Drilling in the Indian Ocean, Geophys. Monogr.*, vol. 70, edited by R.A. Duncan et al., , pp. 387-402, AGU, Washington, D.C., 1992.

Ren, X., Vegetational changes in the past and the uplift of Qinghai-Xizang plateau, in *Geological and Ecological Studies of Qinghai-Xizang Plateau*, edited by B. Gordon, pp. 139-144, Science Press, Beijing, 1981.

Richter, F.M., O.M. Lovera, T.M. Harrison, and P. Copeland, Tibetan tectonics from $^{40}Ar/^{39}Ar$ analysis of a single K-feldpar sample, *Earth Planet. Sci. Lett., 105*, 266-278, 1991.

Robert, C., and H. Chamley, Cenozoic evolution of continental humidity and paleoenvironment, deduced from the kaolinite content of oceanic sediments, *Palaeogeogr. Palaoeclim. Palaeoecol., 60*, 171-187, 1987.

Rögl, F., and F.F. Steininger, Neogene Paratethys, Mediterranean and Indo-Pacific Seaways: implications for the paleobiogeography of marine and terrestrial biotas, in *Fossils and Climate*, edited by P. Brenchley, pp. 171-200, John Wiley, New York, 1984.

Royer, J.Y., and D.T. Sandwell, Evolution of the Eastern Indian Ocean since the Late Cretaceous: Constraints from Geosat altimetry, *J. Geophys. Res., 94*, 13755-13782, 1989.

Ruddiman, W.F., and J.E. Kutzbach, Forcing of the late Cenozoic uplift northern hemisphere climate by plateau uplift in southern Asia and the American West, *J. Geophys. Res., 94*, 18409-18427, 1989.

Ruddiman, W., et al., Late Miocene to Pleistocene evolution of climate in Africa and the low-latitude Atlantic: Overview of leg 108 results, *Proc. Ocean Drill. Program Sci. Results, 108*, pp. 463-484, 1989.

Ruddiman, W.F., J.E. Kutzbach, and I.C. Prentice, Testing the climatic effects of orography and CO_2 with general circulation and biome models, in *Tectonic Uplift and Climate Change*, edited by W.F. Ruddiman, pp. 149-170, Plenum, New York, 1997a.

Ruddiman, W.F, M.E. Raymo, W.P. Prell, and J.E. Kutzbach, The uplift-climate connection: A synthesis, in *Tectonic Uplift and Climate Change*, edited by W.F. Ruddiman, pp. 471-515, Plenum, New York, 1997b.

Sarnthein, M., J. Thiede, U. Pflaumann, U. Erlenleuser, D. Fütterer, B. Koopman, H. Lange, and E. Seibold, Atmospheric and oceanic circulation patterns off northwest Africa during the past 25 millions years, in *Geology of the Northwest African Continental Margin*, edited by U. von Rad et al., pp. 545-603, Springer-Verlag, New York, 1982.

Scott, G.R., Cenozoic surfaces and deposits in the southern Rocky Mountains, *Geol. Soc. Am. Bull., 152*, 227-251, 1977.

Sébrier, M., A. Lavenu, M. Fornari, and J.P. Soulas, Tectonics and uplift in central Andes (Peru, Bolivia and northern Chile) from Eocene to present, *Géodynamique, 3*, 85-106, 1988.

Shackleton, N.J., and N.D. Opdike, Oxygen isotope and paleomagnetic evidence for early northern hemispheric glaciation, *Nature, 270*, 216-219, 1977.

Sirocko, F., Deep-sea sediments of the Arabian Sea: A paleoclimatic record of the southwest Asian summer monsoon, *Geol. Rundsch., 80/3*, 557-566, 1991.

Stewart, J.H., Basin-Range structure in western North America: A review, *Geol. Soc. Am., 152*, 1-31, 1977.

Summerfield, M.A., *Global Geomorphology: An Introduction to the Study of Landforms*, 537 pp., Longman Group, Harlow, 1991.

Sztano, O., Palaeogeographic significance of tidal deposits: An example from an early Miocene Paratethys embayment, northern Hungary, *Palaeogeogr. Palaeoclim. Palaeoecol., 113*, 173-187, 1995.

Tapponnier, P., P. Peltzer, and R. Armijo, On the mechanics of the collision between India and Asia, in *Collision Tectonics*, edited by M.P. Coward and A.C. Ries, *Geol. Soc. Spec. Publ., 19*, 115-157, 1986.

Tapponnier, P., et al., Active thrusting and folding in the Qilian Shan, and decoupling between upper crust and mantle in northeastern Tibet, *Earth Planet. Sci. Lett., 97*, 382-403, 1990.

Traverse, A., Response of world vegetation to Neogene tectonic and climatic events, *Alcheringa, 6*, 197-209, 1982.

Turner, S., C. Hawkesworth, J. Liu, N. Rogers, S. Kelley, and P. Van Calsteren, Timing of Tibetan uplift constrained by analysis of volcanics rocks, *Nature, 364*, 50-54, 1993.

Valdes, P.,*The sensitivity of the Indian summer monsoon to changes in*

orography, paper presented at the EGS XXII General Assembly, Eur. Geophys. Soc., Vienna, Austria, April 21-25, 1997.

Van der Burgh, J., H. Visscher, D.L. Dilner, and W.M. Kürschner, Paleoatmospheric signatures in Neogene fossil leaves, *Science*, *260*, 1788-1790, 1993.

Wang, W.M., Paleofloristic and paleoclimatic implications of Neogene palynofloras in China, *Rev. Palaeobot. Palynol.*, *82*, 239-250, 1994.

Webster, P.J., The elementary monsoon, in *Monsoons*, edited by J.S. Fein and P.L. Stephens, pp. 3-32, John Wiley, New York, 1987.

World Climate Research Program, Simulation and prediction of monsoons: Recent results, *Rep. WCRP-80, WMO/TD - 546*, pp. 27-57, World Meteorol. Organ., Geneva, 1993.

Yin, A., T.M. Harrison, F.J. Ryerson, C. Wenji, W.S.F. Kidd, and P. Copeland, Tertiary structural evolution of the Gangdese thrust system, southeastern Tibet, *J. Geophys. Res.*, *99*, 18175-18201, 1994.

Zubakov, V.A., and I.I. Borzenkova, *Global Palaeoclimate of the Late Cenozoic*, 456 pp., Elsevier, New York, 1990.

J. Besse, and F. Fluteau, Institut de Physique du Globe, Laboratoire de Paléomagnétisme et Géodynamique, URA 729, 4 Place Jussieu, 75252 Paris Cedex 05, France.
(besse@ipgp.jussieu.fr, fluteau@ipgp.jussieu fr).

F. Fluteau, and G. Ramstein, Laboratoire des Sciences du Climat et de l'Environnement, CE-Saclay, Bat 701, 91191 Gif-sur-Yvette, France.
(fluteau@lsce.saclay.cea.fr, ramstin@lsce.saclay.cea.fr).

(Received June 13, 1998; revised December 10, 1998;
accepted December 16, 1998.)